THE RATIONAL DESIGN OF A NOVEL BIOCATALYST USING THE HEME-NITRIC OXIDE/OXYGEN BINDING PROTEIN

A Thesis Submitted to the Graduate School of Engineering and Sciences of Izmir Institute of Technology in Partial Fulfilment of the Requirements for the Degree of
MASTER OF SCIENCE

in Molecular Biology and Genetics

by
Joana Efua AGGREY-FYNN

December 2017
İZMİR

We approve the thesis of **Joana Efua AGGREY-FYNN**

Examining Committee Members:

Asst. Prof. Dr. Gülistan MEŞE ÖZÇİVİCİ
Department of Molecular Biology and Genetics, Izmir Institute of Technology

Asst. Prof. Dr. Nur Başak SÜRMELİ
Department of Bioengineering, Izmir Institute of Technology

Asst. Prof. Gerhard WINGENDER
Department of Immunology and Infectious Diseases,
Izmir Biomedicine and Genome Institute

Asst. Prof Çiğdem Tosun
Department of Molecular Biology and Genetics, Izmir Institute of Technology

Asst. Prof Özden Yalçın Özuysal
Department of Molecular Biology and Genetics, Izmir Institute of Technology

19 December, 2017

Asst. Prof. Dr. Gülistan MEŞE ÖZÇİVİCİ
Supervisor,
Department of Molecular Biology and Genetics
Izmir Institute of Technology

Asst. Prof. Dr. Nur Başak SÜRMELİ
Co-supervisor,
Department of Bioengineering
Izmir Institute of Technology

Prof. Dr. Volkan SEYRANTEPE
Head of the Department of Molecular Biology and Genetics

Prof. Dr. Aysun SOFUOĞLU
Dean of Graduate School of Engineering and Sciences

ACKNOWLEDGEMENTS

My most sincere gratitude goes to my supervisors, Asst. Prof. Dr. Gülistan Meşe Özçivici and Asst. Prof. Dr. Nur Başak Sürmeli for their great support, guidance and patience throughout my graduate studies. I am very blessed to be mentored by two intelligent, disciplined and passionate women.

I am most grateful to Asst. Prof. Dr. Nur Başak Sürmeli for providing everything I needed to complete my studies, for investing in me, helping me grow, supporting me and for being the one of the best professors I have had the pleasure of working with. I wish her the very best in all her endeavors. God bless you hocam.

I would like to express my sincere gratitude to the head of department, Prof. Volkan Seyrentepe, for his assistance, support and understanding during the difficult times of my graduate studies.

Also, I am very thankful to the Özçivici laboratory and the Protein Design laboratory members for their patience, contributions and support. I would also like to thank BIYOMER for all the sequence analyses and the mass spectrometry team at the chemistry department. Finally, I am grateful to Tubitak (grant number 115C134) for sponsoring this project and to Turkiye Burslari for giving me the opportunity to study in Turkey.

My immense gratitude goes to my forever friends, Mariam Muniru, Pamela Aracena Santos, Aikyz Bauyrzhankyzy, Jonathan Kulah, Babrah Dusenge and Cyndy Kiuta, for their immense support and encouragement. Their love and crazy ways were the highlights of my study here in Turkey. Thanks to them, I was able to endure the difficult times and I am eternally grateful.

Finally, I would like to appreciate my foundation, solid rock and inspiration, my family. They never failed to support, defend and uplift me. I especially thank my bestie, daddy, and my love, mommy, for being unique and the best in the world.

“Fear not, for I am with you
Be not dismayed, for I am your God
I will strengthen you, I will help you
And I will uphold you with my victorious right hand”
-Isaiah 41:10

ABSTRACT

THE RATIONAL DESIGN OF A NOVEL BIOCATALYST USING THE HEME-NITRIC OXIDE/OXYGEN BINDING PROTEIN

Recent advances in recombinant DNA technology and protein design have led to the application of biocatalysis as an alternative to chemical catalysis in the synthesis of enantiopure products due to high regio- and enantioselectivity. Hemeproteins are proteins with a heme prosthetic group that play diverse roles in biological systems, making them good candidates for biocatalysis. The Heme-nitric oxide/oxygen binding (H-NOX) protein was identified by homology to the soluble guanylate cyclases. Here, the H-NOX domain from the methyl-accepting chemotaxis protein, *Thermoanaerobacter tencogenesis* (*Tt*H-NOX), was tuned into a biocatalyst using rational design. Four variants of *Tt*H-NOX were cloned, purified and characterized. Each variant was then tested for their catalase and peroxidase activities. The wild type *Tt*H-NOX inefficiently catalyzed the hydrogen peroxide decomposition (catalase activity) and 2,2'-azino-bis(3-ethylbenzthiazoline-6-sulfonic acid (ABTS) oxidation (peroxidase activity). However, the Y140H mutant exhibited an efficient five-fold increase in catalase and peroxidase activities as compared to the wild type. The other mutants, H102Y, H102C and Y140A *Tt*H-NOX, were not good catalysts for both reactions. Therefore, the mutations resulted in changes in reaction rates and electronic properties of the heme group. The mutations affected the molecular mechanism of the hemeprotein, showing that both the proximal and distal pocket residues are vital for catalysis. However, the mutation of the distal tyrosine to histidine of *Tt*H-NOX has significantly improved its catalytic activities. These observations contribute to the understanding of the physiological roles of hemeproteins. This project could also lead to discovery of novel biocatalysts and aid in the design of future biocatalysts.

ÖZET

HEM-NITRIK OKSIT/OKSIJEN BAĞLAYICI PROTEININI KULLANARAK YENI BIR BIYOKATALIZÖRÜN RASYONEL TASARIMI

Rekombinant DNA teknolojileri ve protein tasarımındaki son gelişmeler, biyokatalizörlerin ilaç ve zirai kimyasalların üretiminde kimyasal katalizörlere alternatif olarak kullanılmasına olanak tanıdı. Biyokatalizörler özellikle enzimlerde gözlenen yüksek regio- ve enantio seçimliliklerinden dolayı saf ürünlerin sentezlenmesinde kullanılmaktadır. Biyokatalizörler ayrıca çevre dostudur. Hemoproteinler hem prostetik grubunu içerirler ve biyolojik sistemlerde çeşitli roller üstlenenilir ve biyokatalizör olabilirler. Hem-Nitrik Oksit/Oksijen bağlanan (H-NOK) proteinler nitrik oksit (NO) algılayıcı çözünür guanilat siklaz (sGC) proteini ile homoloji göstermeleriyle kesfedilmişlerdir. Bu projede *Thermoanaerobacter tencogenesis* (*Tt*H-NOK)'in metil-akseptör kemotaksi proteininin H-NOK bölgesi, rasyonel tasarım kullanılarak modifiye edildi. Dört *Tt*H-NOXKvaryantını klonlandı, eksprese edildi, saflaştırıldı ve mutasyonların proteinin spektroskopik ve katalitik özellikleri üzerindeki etkileri incelendi. Her bir varyant daha sonra hidrojen peroksidin (H_2O_2) bozunması ve 2, 2'-azino-bis(3-etilbenztiazolin-6-sülfonk asit) (ABTS)'in oksidasyonu gibi tepkimeler ile test edildi. Doğal *Tt*H-NOK H_2O_2 bozunmasını ve ABTS oksidasyonunu düşük verim ile kataliz etti. Bununla birlikte Y140H mutant en verimli peroksidaz ve oksidaz aktivitelerini gösterdi. Y140H distal mutantı doğal enzimle karşılaştırıldığında katalizde beş kat artış sergiledi. Diğer mutantlar; H102Y, H102C ve Y140A *Tt*H-NOK ilgili reaksiyonlar için iyi katalizörler değillerdi. Bu yüzden, mutasyonlar reaksiyon hızlarında ve hem kofaktörünün elektronik özelliklerinde değişim gösterdiler. Mutasyonlar ayrıca heme proteininin moleküler mekanizmasını etkilediler. Bu sonuçlar proksimal ve distal cepteki amino asitlerin kataliz için önemli olduğunu gösterdi. Bununla birlikte distal tyrosinin histidine mutasyonu enzimin katalitik aktivitesini önemli ölçüde arttırdı. Bu gözlemler hemoproteinlerin fizyolojik rollerini anlamaya katkıda bulunacaktır. Bu proje yeni biyokatalizlerin keşfine ve gelecekte yeni biyokatalizörlerin tasarlanmasına yardım edecektir.

TABLE OF CONTENTS

LIST OF FIGURES

LIST OF TABLES

CHAPTER 1

INTRODUCTION

1.1. Biocatalysis

1.1.1. Overview of Biocatalysis

Enzymes are effective catalysts, which are vital for growth and development of living cells. Enzymes have also been utilized in the production of household, food and medical processes (Bornscheuer and Kazlauskas, 1999). However, despite their potential applications, enzymes have low stability, have substrate specificity and low efficiency. To make them more amenable for industrial purposes, many enzymes from natural sources were screened, random mutations and enzyme immobilizations were attempted (Dincer and Telefoncu, 2007; Elleuche et al., 2014). The accumulation of knowledge in the structures and functions of these enzymes through these processes resulted in the design of enzymes with novel functions, thus the development of biocatalysis (Rothlisberger et al., 2008; Siegel et al., 2010).

Biocatalysis is the use of whole cells or isolated enzymes as catalysts in chemical reactions. Biocatalysts are biological catalysts that speed up the rate of a reaction, do not affect the thermodynamics of the reaction and remain unchanged at the end of the reaction. Biocatalysts have been historically used for the one-step production of aspartic acid, in the multi-step production of alcohol and cheese, (Johannes et al., 2006), the oxidation of ethanol to acetic acid (Wandrey et al., 2000), the production of acrylamide (Asano et al., 1982), the kinetic resolution of amino acids (Tanabe Seiyaku Co. Ltd., 1969) and so on. The range of biocatalytic applications have been increased over the years through the understanding of protein structure and function. The utilization of biocatalysts for chemical processes was possible through the development of design tools such as rational design and directed evolution. Through these processes, tailor-made biocatalysts can be created from wild type enzymes (Bornscheuer and Kazlauskas, 1999).

Today, enzymes with high stability, substrate specificity, selectivity and catalytic activity can be engineered. There are hundreds of biocatalytic processes that are applied in industry; pharmaceutical, food, agrochemical and chemical industries (Pollard and Woodley, 2007).

1.1.2. Advantages and Disadvantages of Biocatalysis

Biocatalysts have unique characteristics. One of the most important characteristic is their high selectivity. Enzymes are stereo-selective (form unequal mixture of stereoisomers), regio-selective (i.e., positional; can differentiate functional groups which are in different regions), and chemo-selective (i.e., functional group specific; pure from impurities) (Bornscheuer and Kazlauskas, 1999). These characteristics are highly desirable and advantageous in chemical synthesis. These characteristics lead to higher yields, fewer side reactions, elimination of protection and de-protection steps, production of pure products, easier recovery and separation. Biocatalytic processes utilize biodegradable catalysis therefore, their processes are "greener" and sustainable. Biocatalysts are enzymes and enzymes are proteins which are biodegradable. Biocatalysts are produced from immobilized enzymes and have also been shown to cause no environmental hazards (Mohammad et al., 2015). Also, biocatalytic processes do not generate waste disposal problems as the use of aqueous solutions lead to reduced solvent consumption. In addition, they require mild operating conditions and low energy input which results in low energy cost thereby leading to lower emissions of greenhouse gases to the environment (Rozzell, 1999). One other advantage is that they can be modified to be more active, stable and selective. These advantages are desirable for industrial and commercial applications (Figure 1.1).

Initially, biocatalysis was not considered a significantly advantageous method in industry so it was not used as the first alternative for biosynthesis. This was because of some perceived limitations and misconceptions surrounding biocatalysis. The first myth was that biocatalytic enzymes required only aqueous solutions to function. This was disproved as many studies have shown that they can also function in non-aqueous environments (Rozzell, 1999).

The second misconception was that biocatalysts are very expensive. Though they are costly due to the cost of production or generation not the enzyme itself but, they can be obtained at reasonable costs. For example, the cost for the production of penicillin G by penicillin amidase is about $1 per kilogram and that for the production of L-aspartic acid by aspartase is less than $0.10 per kilogram (Rozzell, 1999).

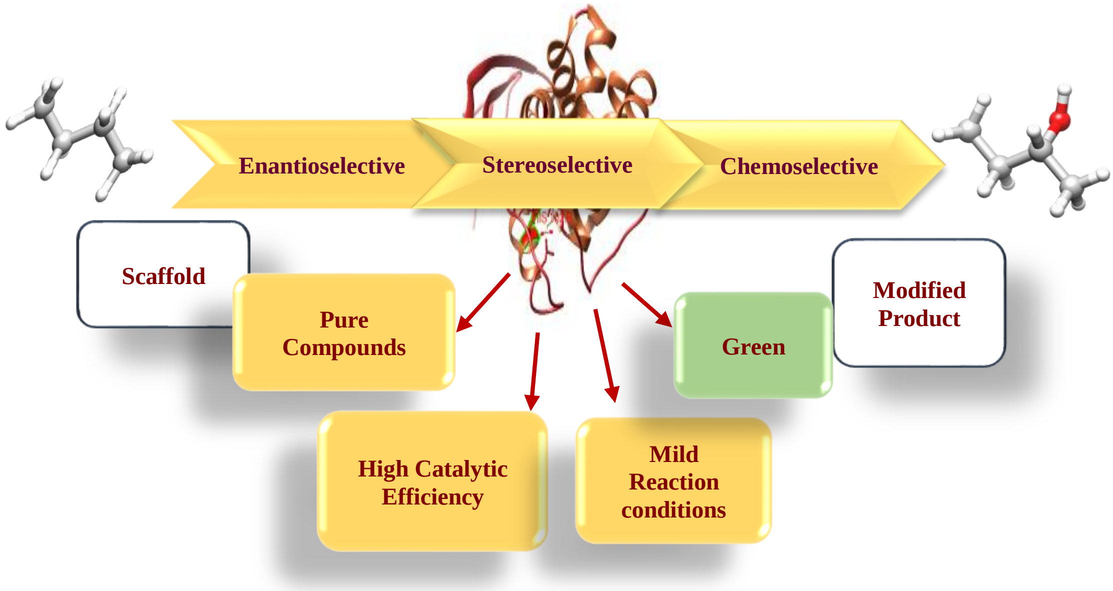

Figure 1.1 Advantages of biocatalysis.

In addition, many believe that at high temperatures and extreme pHs, biocatalysts are unstable. Studies have also shown that many biocatalysts exhibit stability when immobilized through covalent attachment (porous glass, cellulose), adsorption (DEAE-cellulose), entrapment (polymeric gels), encapsulation (hollow fibers, microcapsules) and intermolecular cross-linking (aliphatic diamines, dimethyl suberimidate) (Spahn and Minteer, 2008) (Kadnikova and Kostic, 2002; Homaei et al., 2013). Additionally, thermostable biocatalysts can be developed through their isolation from thermophilic vectors or by their design through protein engineering for example, fungal cellulase (Trudeau et al., 2014) and thermostable terpene synthase (Diaz et al., 2011). Also, there are many examples of enzymes with a long half-life; aspartase has a half-life of 6 months to 2 years (Crump and Rozzell, 1992) and that for isomaltulose synthase is 358 days (Lee and Henthorn, 2012).

Also, it has been assumed that biocatalysis has low productivity. This misconception was due to the fact that the fermentation processes have low volumetric productivities, usually less than 1 gram/liter/hour (Rozzell, 1999). This was because the fermentation process involved a pathway of carbon precursors. However, high productivities have been increased through the immobilization of enzymes (Homaei et al., 2013; Mohamad et al., 2015). Examples are the production of 1-phenylethylamine by lipase-catalyzed acylation and L-aspartic acid by immobilized aspartase (Rozzell, 1999).

One other limitation is the misconception that redox cofactors such as nicotinamide cofactors involved in biocatalysis are difficult to recycle. However, cofactors have been successfully recycled using different methods. One of such method is the use of a coupled reaction. A reaction where the catalysis of the synthesis of a product from one substrate and the cofactor regeneration reaction with a second substrate is done by an enzyme which utilizes the reduced and the oxidized forms of that cofactor (Lemiere et al., 1985). An example is the production of phenyllactic acid from the reduction of phenyllactate dehydrogenase using nicotinamide adenine dinucleotide (NADH). NADH is regenerated using alcohol dehydrogenase and ethanol (Rozzell, 1999; Liu and Wang, 2007). The second is the use of a macro-molecularized cofactor in a membrane reactor such as the flat-membrane, hollow-fibre and packed-bed reactors (Liu Liu and Wang, 2007). The NAD^+ cofactor has been recycled using this method. The third method is the use of whole cells and a carbon source. Here, whole cells with dehydrogenase enzymes and a cofactor are used. The cofactor is then recycled through the addition of a carbon source. The carbon source provides reducing equivalents for the degeneration of the cofactor and maintenance energy to the cell (Servi, 1990).

Finally, it is also a misconception that biocatalysis can only produce one or two possible enantiomers (Shoemaker et al., 2003). However, studies have shown that biocatalysts can convert a racemic mixture to a new product with different chemical and physical properties which can be separated through the appropriate separation method (Liese et al., 2002; Schmid et al., 2001).

Biocatalysis have limitations however, these have become their strengths. These strengths have made biocatalysis an important tool in the industrial synthesis of bulk chemicals, agrochemical intermediates, pharmaceuticals, and food ingredients. Since we are limited by enzymes, the need for more biocatalysts with novel functions is imperative. Therefore, this study seeks to create an effective novel biocatalyst with peculiar chemical and physical characteristics which would contribute to the world of biocatalysis.

1.2. Hemeproteins

Heme is one of the most important coenzymes and a widely used metalloprophyrin in nature. All hemeproteins carry iron (Fe) protoporphyrin IX as a prosthetic group and can catalyze both reductive and oxidative chemistry (Poulos, 2014).

The heme consists of an Fe ion bound to four central nitrogen atoms of a porphyrin ring as seen in figure 1.2. One or two axial ligands which are different between hemeproteins at the iron (Fe) ion gives a complete octahedral coordination (Rydberg et al., 2004). There are two common types of heme, heme b and heme c (Figure 1.2). Heme b forms a noncovalent bond to proteins while heme c forms covalent bond between the vinyl groups and cysteine residues of proteins (Li et al., 2011).

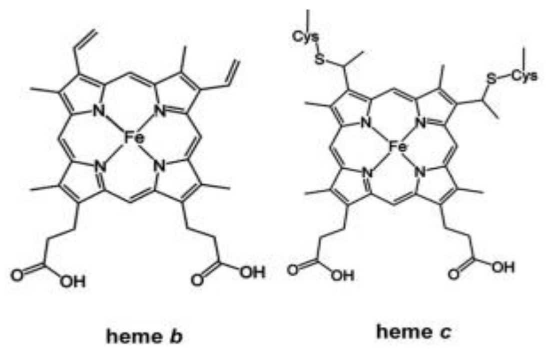

Figure 1.2 Structures of heme b and c (Source: Li et al., 2011).

Hemeproteins have diverse roles in oxygen transport (hemoglobin and myoglobin) (Antonini and Brunori, 1971; Olson et al., 1999; Wittenberg and Wittenberg, 1990), electron transfer (cytochrome b5) (Moore and Pettigrew, 1990) and in catalytic reactions (NO synthase, cytochrome P450, catalase, NO reductase and so on) (Isaac and Dawson, 1999; Jouve et al., 1997; Park et al., 1997). Some hemeproteins play a role to sense gaseous, diatomic small molecules like carbon monoxide (CO), nitric oxide (NO) and oxygen (O_2) (Pellequer et al., 1999; Jain and Chan, 2003). Four heme-based sensors have been identified based on their heme-binding domains. They are classified on the basis of their ligand specificity and functionality to sense either CO, NO or O_2. Two domains found in prokaryotes are specialized for O_2 sensing. The first is the myoglobin-like heme domain which is contained in an aerotaxis-regulating protein, HemAT (Hou et al., 2000; Aono et al., 2002). The second is the heme-PAS domain found in the histidine kinase containing protein, FixL (Gilles-Gonzalez et al., 1991; Monson et al., 1992). The third heme domain is carbon monoxide (CO) sensing found in *Rhodospirillum rubrum* CooA protein which regulates the genes involved in CO oxidation (Shelver et al., 1997). The last domain is a nitric oxide (NO)-sensing domain found in soluble guanylate cyclases (sGCs) (Jain and Chan, 2003).

Two common hemeproteins are peroxidases and catalases. Peroxidases catalyze 1-electron oxidation of a variety of substrates using hydrogen peroxide. The first step of the catalytic oxidation yields a compound I, a ferryl porphyrin cation radical (Fe^{IV} = $OPor^{\bullet+}$). Compound I is then reduced to the ferric compound II, ferryl porphyrin (Fe^{IV} = OPor) (Matsui et al., 1999). Compounds I and II are known as the heme iron intermediates and are produced from a heterolytic and hemolytic reaction cycle with the ferric heme as the final product (Gumiero et al., 2011) (Figure 1.3). Catalases catalyze the decomposition of hydrogen peroxide to water and oxygen in two steps producing compounds I and II respectively (Boon et al., 2007).

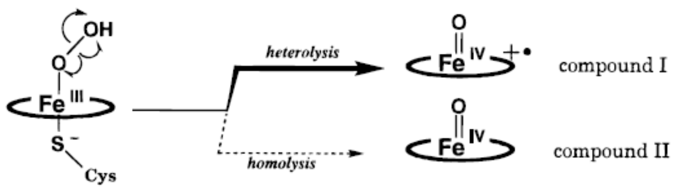

Figure 1.3 Mechanism of compound I and II formation in cytochrome P450. (Source: Matsui et al., 1996).

The amino acid residues surrounding the heme prosthetic group, iron protoporphyrin IX, play very important roles in the function of the heme. The amino acid residues at the axial ligands of heme varies so does their functions. Globins have only one histidine ligand but the distal side has a water molecule which is open for oxygen binding (Kaim and Schwederski, 1996; Liddington et al., 1992). Cytochrome P450s (Li H., 2001), chloroperoxidases (Sundaramoorthy, 2001) and NO synthases (Rosenfeld, 2001) have cysteine heme ligands. Figure 1.4. shows the axial and distal pockets of the heme active site.

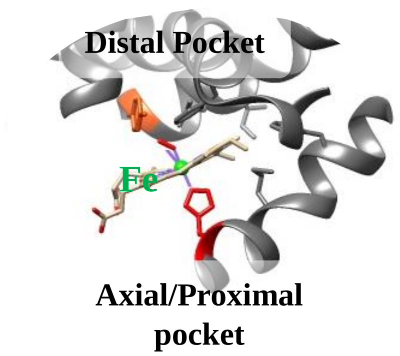

Figure 1.4 The active site of a heme protein showing the distal and proximal binding sites.

All peroxidases have a histidine ligand (Gajhede, 2001) while all catalases have a tyrosine ligand (Maté et al., 2001). Heme also have a second set of ligands called the distal ligands which varies among hemeproteins. In peroxidases, the proximal histidine ligand forms a hydrogen bond to an aspartate residue (Gajhede, 2001), increasing the electron density on the Fe ion (Poulos, 1996). In globins, the histidine ligand has a weak hydrogen bond to the backbone of carbonyl groups (Kaim and Schwederski, 1996) and catalases have a tyrosine ligand which forms a hydrogen bond with arginine (Maté et al, 2001). The roles of the axial and distal residues of some hemeproteins on function and activity have been studied.

In addition, it has been shown that the axial or proximal ligand have a "push-pull" effect. The ligand, "the push", stabilizes the oxidation state of compounds I and II through its hydrogen bond to the aspartate residue which increases the negative charge of the ligand and the charge density of the Fe (Green, 2000). The reactivity, "the pull", is from the distal side where the histidine and arginine residues enhances heterolytic reactivity (Rydberg et al., 2004). For example, cytochrome P450 has a stronger "push" because there are no distal side residues. Therefore, axial ligand residues have an effect on the reduction potentials thereby stabilizing compounds I and II but have no effect on the hemolytic O-O bond cleavage (Poulos, 1996).

1.2.1. Cytochrome P450

Cytochrome P450s (CYPs) are heme b containing monooxygenases which catalyze regio- and stereospecific oxidations of non-activated hydrocarbons under mild reaction conditions (Urlacher and Girhard, 2012). In the CO-bound reduced form, they have a maximum absorption at 450 nm, giving their name, cytochrome P450. CYPs are very important for allowing microorganisms to live on particular carbon sources such as acetate and pyruvate. (Bradshaw and Conrad, 1959). They are also involved in mammalian biological processes such as those involved in growth, development, homeostasis, and production of compounds for defense (Zerbe et al., 2002; Lamb and Guengerich, 2006). They exhibit low specificities thereby, providing a general defense against harmful products such as terpenes and alkaloids (Isin and Guengerich, 2007). CYPs catalyze oxidation and atypical reactions such as *N*-oxidation, aromatic hydroxylation, epoxidation of C=C double bonds, *N*-, *O*- and *S*-dealkylation deamination and dehalogenation (Urlacher and Girhard, 2012). Atypical reactions include cleavage of C-C bonds (Shyadehi et al., 1996), Baeyer-Villiger oxidation (Isin and Guengerich, 2007), C-C and C-O phenol coupling (Zerbe et al., 2004) and rearrangement reactions (Ortiz de Montellano and Nelson, 2011). There are more than 7000 CYPs and their chemical characteristics; low substrate specificity, atypical kinetics and versatile nature make then good candidates for biocatalysis in biotechnology, bioremediation and medicine (Kumar, 2010) (Figure 1.5).

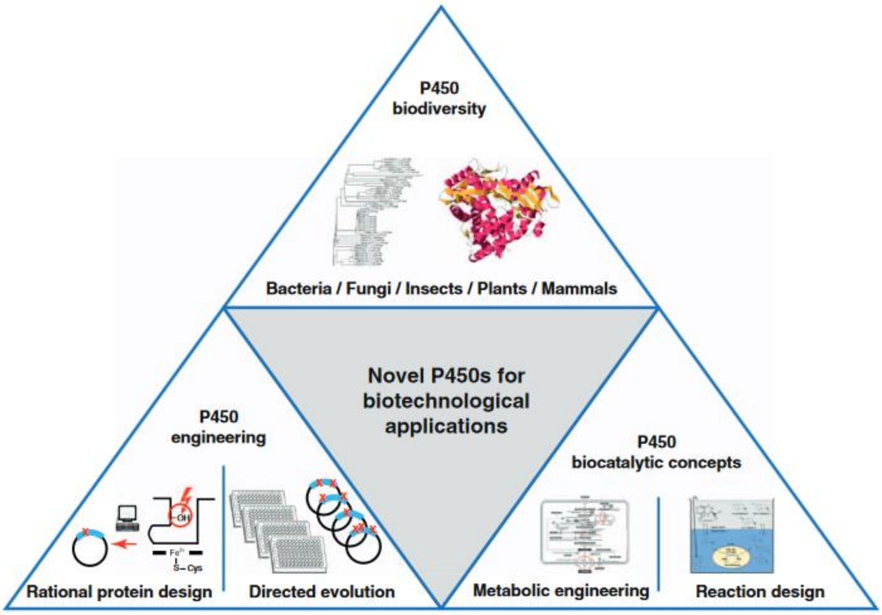

Figure 1.5 Biocatalytic routes to the design of novel CYPs (Source: Urlacher and Girhard, 2012).

P450s have been utilized in the production of drug, drug metabolites and steroids (Urlacher and Girhard, 2012). One commercial application is the production of steroids for example, the production of hydrocortisone for 11β-hydroxylation of Reichstein compound S by *Curvularia sp* (Sonomoto et al., 1983), pravastatin from compactin using *E. coli* (Fuji et al., 2009), the production of leukotoxin B, eicosanoid epoxides and epoxyeicosatrienoic acid from CYP 102 (Falck et al., 2001). CYPs are also used in dyes, pesticides and in horticulture where CYP genes are transferred from other plants to create flowers of unique colors (Gillam and Guengerich, 2001).

Gene-Directed Enzyme Prodrug Therapy (GDEPT) has been used for cancer treatments through the CYP-based activation of chemotherapeutic prodrugs by increasing the chemosensitivity of tumor cells (Kumar, 2010). GDEPT has been shown to decrease or eliminate the toxic metabolites and the toxicity of high doses of prodrugs (Chen and

Waxman, 2002; Roy and Waxman, 2006). Examples of chemotherapeutic prodrugs that have been developed include cyclosphosphamide (CPA) and ifosfamide (IFA). CYP2C18 and CYP3A4 have been shown to have strong cytotoxicities to CPA and IFA respectively (Jounaidi et al, 1998; Jounaidi and Waxman, 2004). Human CYP2B6 has been shown to improve antitumor activity (Jounaidi and Waxman, 2001) and cause cell death (Hunt, 2001) through the activation of CPA. Another medical application is their biotransformation into biosensors to monitor drug levels since genetic variations lead to different drug responses. CYP biosensors are also used to detect food contaminants (Bistolas et al., 2005).

In bioremediation, Polycyclic Aromatic Hydrocarbons (PAHs), Polychlorinated Dibenzo-p-dioxins (PCDDs) and polychlorinated biphenyls (PCBs) are metabolized by CYP enzymes (Ishaq et al., 2003). CYP101, 102, 1A1, 1A2 and 1B1 have been used to metabolize PAHs (Isin and Guengerich, 2007). Recombinant cells have been successfully utilized to express CYP1A1 and F240A for the degradation of PCDDs (Sakaki et al., 2002; Shinkyo et al., 2006). In addition, bacterial and plant CYP enzymes are used to remove herbicides by converting them to less lipophilic and toxic metabolites (Morant et al., 2003).

CYP biocatalysts with novel activities were engineered using rational approach, semi-rational approach (CYP2B family enzymes) (Zhao and Halpert, 2007), Conserved Sequence Motif (CSM) analysis (CYP2 family) (Oezguen et al., 2008) and directed evolution (Woycechowsky et al., 2007). Most engineered CYPs are bacterial CYPs and mammalian CYPs. For bacterial CYPs, CYP102 has been studied the most (by directed evolution) as a biocatalyst (Joo et al., 1999). CYP101 has also been engineered through site-directed mutagenesis where the mutants are very efficient at oxidizing PCBs, PAHs and so on through the reductive dehalogenation of hexachloroethane and pentachloroethane (Walsh et al., 2000). Engineered mammalian CYPs, CYP1A2 and 2A6, have been used for xenobiotic reactions as their abilities to catalyze 7-methoxyresorufin O-demethylation (Kim and Guengerich, 2004), 7-methoxycoumarin O-demethylation, tert-butyl methyl ether O-demethylation and indole 3-hydroxylation have been shown (Kim and Guengerich, 2005).

1.2.2. Heme-Nitric Oxide/Oxygen (H-NOX) binding domain

Nitric oxide (NO) is a free radical and an important signalling molecule. NO signalling has diverse physiological roles in the cardiovascular system (vasodilation, platelet aggregation), nervous system (neurotransmission), immune system (eradication of pathogens) and reproduction (egg fertilization) (Denninger and Marletta, 1999) (Hare and Colucci, 1995) (Shah and MacCarthy, 2000; Toda and Okamura, 2003). In order to perform such functions, NO interacts with the sensitive receptor, soluble guanylate cyclase (sGC). sGCs are heterodimeric heme sensors that selectively and actively bind to NO at the ferrous ion. This binding activates the enzyme to convert guanosine triphosphate (GTP) to cyclic guanosine monophosphate (cGMP). cGMP, a secondary messenger, in turn mediates the downstream signalling events; cGMP-dependent calcium ion (Ca^{2+}) channels, kinases and phosphodiesterases (Underbakke and Surmeli, 2013). sGC selectively binds to NO even at high oxygen concentrations even though the heme is identical to that of the proximal histidine ligand globin proteins. Therefore, even a weak oxygen binding to the heme will lead to the blockage of the entire NO signalling pathway (Boon and Marletta, 2005). The binding of sGC to NO leads to the dissociation of the proximal histidine residue, forming a 5-coordinate (5C) active complex. In bacteria, NO signalling controls bacterial communal behaviour, symbiosis, biofilm formation and disintegration, motility and quorum sensing (Plate and Marletta, 2012; Carlson et al., 2010; Henares et al., 2012; Wang, 2010).

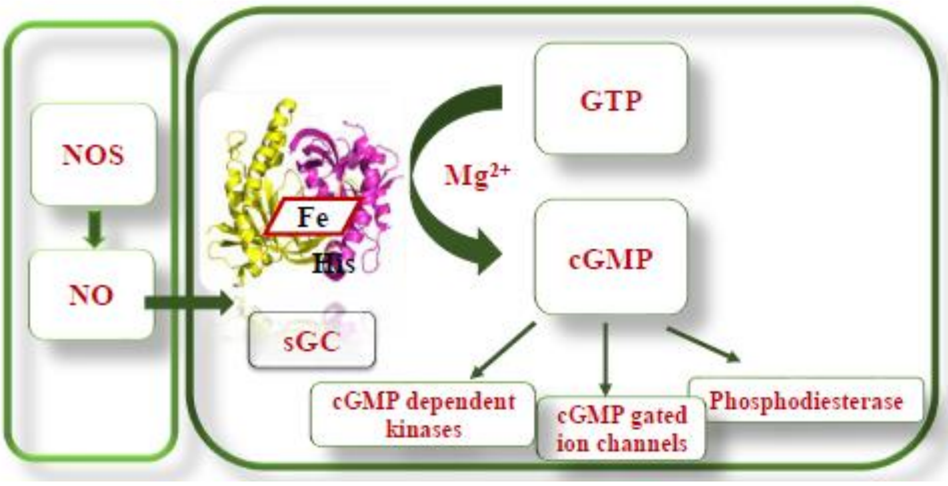

Figure 1.6 NO activates sGC which converts GTP to cGMP. (NOS → NO synthase).

A new family of prokaryotic hemeproteins with 15-40 % sequence homology to eukaryotic sGC were discovered in 2003 (Iyer et al., 2003; Schmidt et al., 2004; Karow et al., 2004). These proteins were discovered in different facultative aerobes across the *Bacteriodates, Cyanobacteria, Thermotagae, Proteobacteria* and *Firmicutes* phyla (Iyer et al., 2003; Karow et al., 2004). These heme domains have a high sequence identity to sGC and a conserved Y-S/T-R heme binding motif (Schmidt et al., 2004; Schmidt et al., 2005) as seen in Figure 1.7. After cloning and spectroscopic studies, these heme domains excluded oxygen as a ligand and formed a 5-coordinate complex with NO just like sGC (Karow et al., 2004). This family was named the Heme-Nitric Oxide/Oxygen (H-NOX) binding domain.

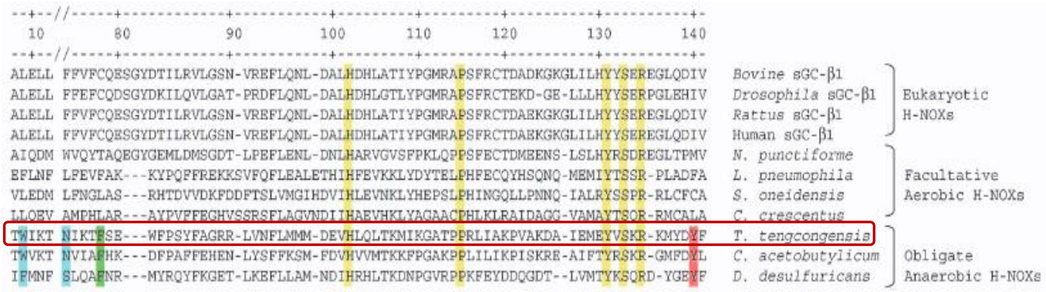

Figure 1.7 Sequence alignments of selected eukaryotic and prokaryotic H-NOX proteins. Yellow: Conserved residues across all H-NOX proteins. Red: Tyrosine residue required for oxygen binding in H-NOX proteins. Blue: Tryptophan 9 and Asparagine 74 residues in obligate anaerobes. Green: Phenylalanine 78 residue. Black: Obligate anaerobic H-NOX sequences. Orange: Facultative aerobics H-NOX sequences. Purple: Eukaryotic H-NOX sequences. Source: (Source: Boon and Marletta, 2005).

The hemeprotein from a family of obligate anaerobe, *Thermoanaerobacter tencogenesis*, was shown to have similarities with the globin proteins that forms a stable oxygen complex and a 6-coordinate NO complex (Karow et al., 2004). It has been suggested that H-NOX proteins in obligate anaerobes have evolved to bind to oxygen (i.e. not exclude oxygen) as a ligand whereas the rest only selectively bind NO. The amino acid residues surrounding the heme are responsible for this ligand discrimination. Therefore, specific amino acid changes through protein design will explain the molecular mechanisms for ligand selection (Boon and Marletta, 2005).

1.2.2.1. *Thermoanaerobacter tencogenesis* H-NOX (*Tt*H-NOX) sensing proteins

Pellicena *et al*, reported the structure of the oxygen-binding H-NOX domain from the thermophilic anaerobe, *Thermoanaerobacter tencogenesis,* (*Tt*H-NOX) (Pellicena et al., 2004). *Tt*H-NOX has seven α-helices, four-stranded antiparallel β-sheet (Figure 1.8a) and a hydrogen-binding network around the bound ligand, oxygen. This network involves the phenol of tyrosine-140 (Y140) bound to O_2 and asparagine-74 (N74) and tryptophan-9 (W9) bound to the phenolic O_2 of Y140 (Figure 1.8b) (Boon and Marletta, 2005).

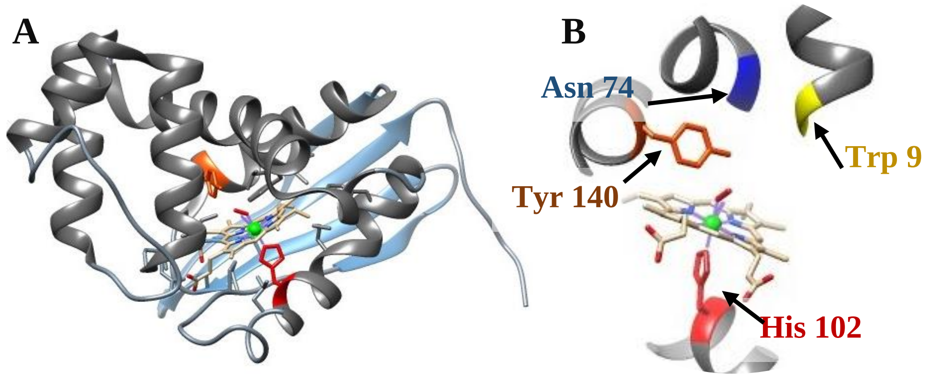

Figure 1.8 The structure of *Tt*H-NOX. (A) *Tt*H-NOX has 7 α-helices and four β-sheets. (B) The ligand-binding pocket of *Tt*H-NOX showing the hydrogen bond network and the O_2-bound iron protoporphyrin IX.

Extensive studies on *Tt*H-NOX through mutagenesis has revealed some unique molecular characteristics of the ligand-binding pocket. These include, heme distortion (distorted heme cofactor due to a conserved proline and isoleucine residues), heme pocket conformation (Olea et al., 2008), protein dynamics and a ligand entry and exit tunnel network which influence ligand specificity (Plate and Marletta, 2013). Also, the presence of the distal residue, Y140, which plays an important role in O_2/NO ligand discrimination. A Y140 to leucine *Tt*H-NOX mutant provided evidence that the Y140 residue is responsible for O_2/NO ligand discrimination and the formation of stable O_2 complexes in sGCs using a kinetic selection (Boon and Marletta, 2005). The distal tyrosine provided a hydrogen bond network around the heme, modulating O_2-binding affinity in the heme. Without the distal Y140, the dissociation rate for O_2 in much faster thus, making it responsible for ligand discrimination in H-NOX family (Boon and Marletta, 2005).

1.3. Design of Hemeproteins

1.3.1. Rational Protein Design

Protein design is a technique which involves the creation novel functional proteins through the use the specific structure and sequence of the original protein. Rational protein design uses computational tools which assist in designing and engineering proteins to identify functional mutations. This technique requires every information about the enzyme, structure, mechanism and function. Amino acids substitutions are selected and single point mutations which can cause structural and functional changes are made. Therefore, it is important that the wild type and mutant enzymes are compared in order to ensure that the mutation is site-directed (Bornscheuer and Pohl, 2001). In contrast, directed evolution is a technique to "evolve" proteins through random mutagenesis like error-prone PCR or gene recombination to generate libraries which are assayed to identify variants with improved chemical characteristics (Bornscheuer and Pohl, 2001). The designed and engineered proteins obtain desired catalytic properties which improve catalytic efficiency of the end product biocatalysts (Tiwari et al., 2012). Catalytic properties include the change of substrate specificity, cofactor specificity, enantioselectivity, stability, enzyme mechanism and increase in the promiscuity of the enzyme which are useful strategies to reinforce improved enzymes (Cedrone and Menez, 2000; Harris and Craik, 1998). Though the designed enzymes are functional, their efficiency is many magnitudes lower than that of the natural catalysts (Wolfenden and Snider, 2001).

Rational design by site-directed mutagenesis (SDM) involves planned mutations on the basis of the proteins structure. After transformation in the host organism, the variant is expressed, purified and analyzed for desired properties. This approach is repeated until desired biocatalysts are generated (Figure 1.9).

1.3.2. Rational Design of Hemeproteins

Myoglobin (Mb) is an O_2 binding cytoplasmic hemeprotein responsible for the transport of oxygen molecules to muscle tissues. The heme pocket of myoglobin has a proximal histidine-93 (H93), a distal histidine-64 (H64) and a hydrogen bond network in the heme pocket (Guo et al., 2012). Mb has been used as a scaffold for rational protein design to create functional proteins (Watanabe et al., 2007; Lu et al., 2001; Lu et al., 2009; Pfister et al., 2005). By re-designing the heme active site, Mb has been successfully converted to peroxidases (Matsui et al., 1999; Matsuo et al., 2011; Sato et al., 2004), heme-copper oxidases (Sigmam et al., 2003) and nitric oxide reductases (NOR) (Lin and Yeung et al., 2010; Lin et al., 2010).

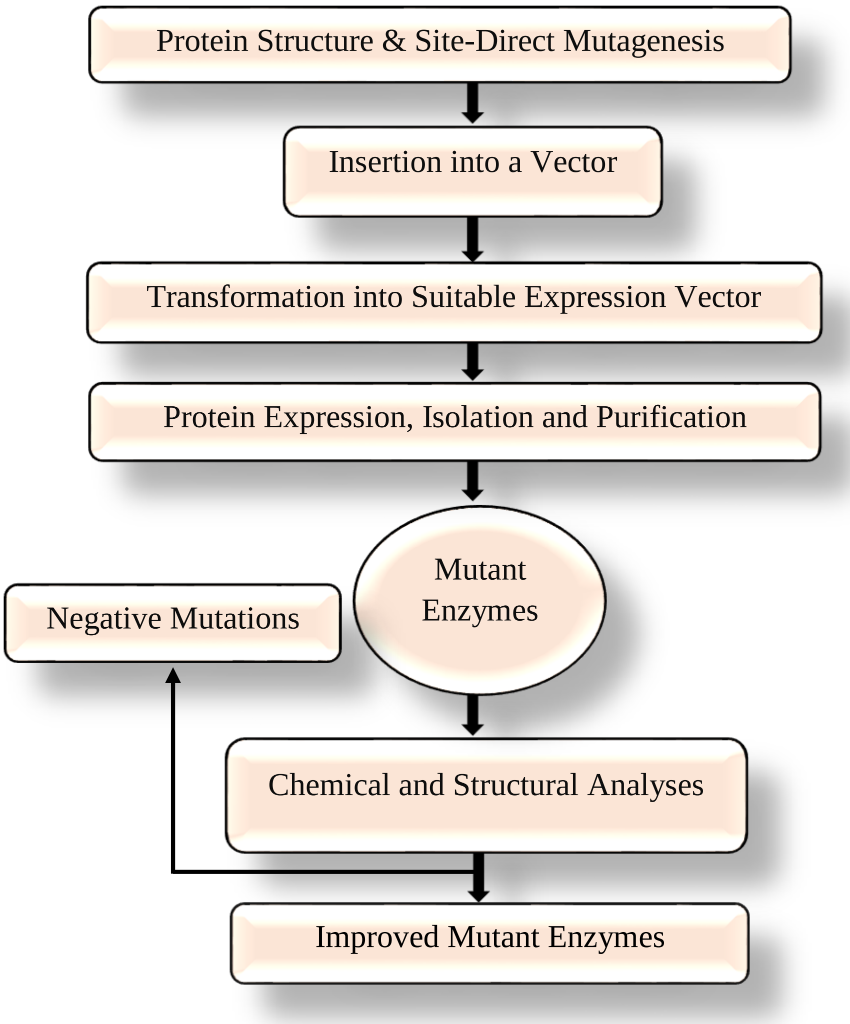

Figure 1.9 Rational protein design approach.

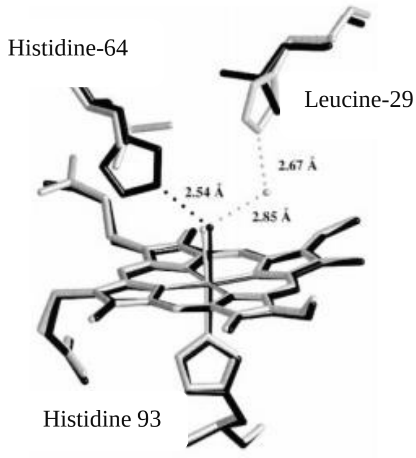

Figure 1.10 The heme pocket of sperm whale myoglobin (Source: Lin et al., 2010).

The role of copper and protons in heme-copper oxidase (HCO) were also investigated by site-directed mutagenesis of Mb. Here double mutations were done to mimic the HCO. Leucine-29 to histidine/phenylalanine-43 to histidine (L29H/F43H) mutant generated a verdoheme instead of a ferryl-heme, due to the lack of the hydrogen bonding network, decreasing the O_2 affinity of the heme. However, the addition of silver (I), Ag(I), increased the O_2 binding affinity. This study explained the importance of the copper center in O_2 binding and reduction, promoting HCO activity (Sigmam et al., 2003).

Recently, the 2-Histidine-1-Glutamate conserved metal center of nitric oxide reductase (NOR), a non-heme iron-containing enzyme was successfully engineered in swMb. Three mutations on the swMb; L29 to glutamate, F43 to histidine, and a no histidine 64 mutant (Fe_BMb(-His)) were made. The Fe_BMb(-His) mutant bound to copper, iron and zinc and exhibited NOR activity (Lin et al., 2010). A functional bacterial NOR was designed by the introduction of two glutamate and three histidine residues into the swMb. The valine-68 to glutamate mutant (V68E) which has three histidine residues and one glutamate bound to iron making the heme pocket similar to that of NOR (Yeung et al., 2009) (Figure 1.11).

Based on the work done on CYPs and Mb, the re-design of *Tt*H-NOX proteins will be attempted. The wild type and variants of *Tt*H-NOX will be tested and characterized for their abilities to catalyze the decomposition of hydrogen peroxide (catalase activity), oxidization of 2,2'-azino-bis(3-ethylbenzthiazoline-6-sulfonic acid) (ABTS).

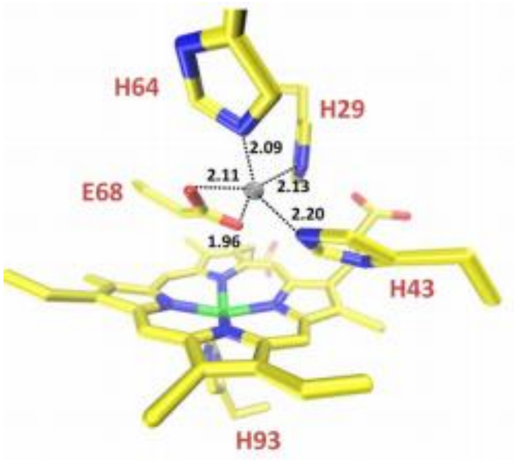

Figure 1.11 The active pocket for non-heme iron-binding enzymes showing three histidine and one glutamate residues (Source: Yeung et al., 2009).

1.4. Scope of this Study

In this study, the H-NOX protein from the thermophilic anaerobic bacteria, *Thermoanaerobacter tencogenesis*, is used as a scaffold for rational protein design through site-directed mutagenesis. Amino acid mutations on the heme active pocket will create mutants with different structural and chemical characteristics. The isolation and purification will be the first step in the characterization and comparisons of the mutant and wild type proteins. The proteins obtained will be tested for potential catalytic activities. The catalytic activity towards decomposition of hydrogen peroxide and oxidation of ABTS by the wild type protein and mutants will be compared. The selected manipulations on the H-NOX protein are imperative for the elucidation of the mechanisms for hemeprotein substrate interactions, the roles of the heme pocket amino acids on protein function and will also aid in the rational design of future biocatalysts. This study will contribute to the understanding of hemeproteins like sGCs and lead to the discovery of novel biocatalysts. Therefore, experiments were performed to express and purify wild type H-NOX from *Thermoanaerobacter tencogenesis* and its variants. Their physical and chemical properties were characterized using UV-Vis spectroscopy and chemical reactions. The chemical and kinetic characterizations were performed through the measurement of catalase activities on hydrogen peroxide and peroxidase activities through the oxidation of 2,2'-azino-bis(3-ethylbenzthiazoline-6-sulfonic acid).

CHAPTER 2

MATERIAL AND METHODS

A. Wild Type (WT) and Mutant H-NOX Heme Protein from *Thermoanaerobacter tencogenesis* (*Tt*H-NOX).

Planned HNOX Mutations:

a) Proximal Mutations: H102C (histidine-102 to cysteine) and H102Y (histidine-102 to tyrosine)
b) Distal Mutations: Y140A (tyrosine-140 to alanine), and Y140H (tyrosine-140 to histidine).

Plasmid: pET-20b (With T7 Promoter and Histidine Tag Coding Sequence).
Cloning Cells: DH5α Competent Cells.
Expression Vector: BL21 DE3 Competent *E. coli* Cells.
Media for Cell Growth: Lysogeny Broth (2 g LB in 100 ml deionized water) and Agar Media (8 g LB and 6 g agar in 0.4 L deionized water).
Media for Large Scale Expression: Terrific Broth containing 6 g tryptone, 12 g yeast extract, 2 ml 100 % glycerol, 50 ml KH_2PO_4-K_2HPO_4 mix in 450 ml deionized water.
Amino Acid Sequences: Appendix A.

2.1. Cloning, Bacterial Transformation, Plasmid Purification and Sequence Confirmation

The *Tt*H-NOX gene sequence in pET20b with a C-terminal histidine tag was obtained thanks to the Marletta Laboratory at the University of California (Berkeley, United States). The cloning was achieved by site-directed mutagenesis using the Q5 Site Directed Mutagenesis Kit (BioLabs). The sequence of interest was exponentially amplified by Polymerase Chain Reaction (PCR) using the forward and reverse primers shown in Table 2.1. The PCR conditions are shown in Table 2.2. In order to treat and enrich the sequence, the Kinase-Ligase-DpnI (KLD) enzyme mix reactions were performed for five minutes at room temperature to remove the template and allow rapid circularization into plasmids (Table 2.3). The plasmids were then transformed into competent DH5α cells with heat shock bacterial transformation protocol. The transformed PCR products were incubated on ampicillin-LB-agar plates at 37 ^{o}C overnight.

Table 2.1. Forward and reverse primer sequences.

Mutant	Forward Primer Sequences	Reverse Primer Sequences
H102C	5'-GGATGAAGTGtgtCTGC AGCTGAC-3'	5'-ATCATCATCAGAA AGTTCACC-3'
H102Y	5'-GGATGAAGTGtatCTGC AGCTGA-3'	5'-ATCATCATCAGAA AGTTCACCAG-3'
Y140A	5'-AATGTATGATgctTTTC TGGGCCTGATTG-3'	5'-TTACGTTTGCTC ACATATTC-3'
Y140H	5'-AATGTATGATcatTTTC TGGGCC-3'	5'-AATGTATGATGAGTT TCTGGGCC-3'

Table 2.2. PCR reaction conditions.

Step	Temperature (^{O}C)	Time (seconds)
Initial Denaturation	98	30
25 Cycles	98	10
	58	30
	72	30
Final Extension	72	120
Hold	4	∞

Table 2.3. KLD reaction conditions.

	10 µL Reaction	Final Concentration
PCR Product	1 µl	
2x KLD Reaction Buffer	5 µl	1X
10x KLD Enzyme Mix	1 µl	1X
Nuclease-Free Water	3 µl	

To isolate plasmids from DH5α cells, about 5 ml cultures were prepared in LB media with 50 mg/ml ampicillin under sterile conditions for selected DH5α colonies (six colonies on average). The plasmids were then isolated using the Macherey-Nagel kit for DNA Purification. was used. About 50 µl pure plasmids were isolated for each sequence variant. Their concentrations and purity of the plasmids were determined using a NanoDrop Spectrophotometer. In order to confirm the success of the site-directed mutagenesis and the presence of the WT and mutants, purified plasmids were sent to the Biotechnology and Bioengineering Research and Application center, Izmir Institute of Technology for sequence analysis. The sequences were confirmed with the GENEIOUS sequence alignment program. Sample plasmids with confirmed wild type and mutated sequences were stored in -80 ^{o}C in 50 % glycerol stocks.

To test for *Tt*H-NOX protein expression, wild type and mutant plasmids were transformed into the expression vector, competent BL21 (DE3) and plated on LB plates containing 50 mg/ml ampicillin. Selected colonies were prepped for small scale expression by incubating in LB broth overnight at 37 ^{o}C.

2.2. Expression of WT and Mutant *Tt*H-NOX Proteins

About 10 ml of LB media with 100 µg/ml ampicillin solutions were prepared (for each colony) and inoculated with 100 µl overnight cell cultures. These were incubated at 37 ^{o}C until the absorbances at 600 nm (OD_{600}) were between 0.5-0.6. About 1 ml of the cells (time, T=0) were collected at this time, pelleted to remove supernatant and frozen at -80 ^{o}C. In order to induce expression, Isopropyl β-D-1-Thiogalactopyranoside (IPTG) solutions with a final concentration of 0.5 mM was added to each culture left to incubate for 1 hour at 37 ^{o}C with shaking at 220 rpm. The OD_{600} after 1 hour (time, T=1) were measured and normalized volumes (from absorbance measurements) were pelleted and stored at -80 ^{o}C. The remaining cultures were incubated overnight (time, T= overnight) at 25 ^{o}C, OD_{600} of diluted cells were measured, cells were pelleted and stored at -80 ^{o}C.

2.3. SDS-PAGE Analysis

Sodium Dodecyl Sulfate Polyacrylamide Gel Electrophoresis (SDS-PAGE) was employed to analyze the success of *Tt*H-NOX protein expressions according to their molecular weight throughout the study. In order to do this, the pelleted cells (T=0and T=1 for each sample) from the small scale protein expression analysis were prepped with SDS loading dye (100 mM Tris-Cl, 4 % SDS, 0.2 % bromophenol blue, 20 % glycerol) and 1 mM dithiothreitol (DTT). The samples were heated up to approximately 95 ^{o}C and loaded into the polyacrylamide gel. SDS denatured and applied the negative charge on the proteins making them linear. DTT reduced the sulfide bonds in the protein structure thereby, unfolding the structures of the proteins. The linear, negatively charged proteins were separated based on their molecular weights through the electric field that is supplied through the gel. The higher molecular weighted proteins moved slower than the low weighted ones. A 250 kDa protein ladder was used to identify the protein sample by its size, about 26 mbp. The gel was stained using the Coomasie Brilliant Blue dye.

2.4. Isolation and Purification of WT and Mutant *Tt*H-NOX Proteins

2.4.1. Large Scale Expression

To produce a significant amount of each protein variant, 1 L large scale protein expressions assays were performed. From the glycerol stocks, 100 ml overnight cultures of the variants with confirmed sequences were prepared in sterile ampicillin-LB broths. About 1 L autoclaved terrific broths containing KH_2PO_4-K_2HPO_4 mix with 0.1 mg/ml ampicillin were inoculated with 5 ml overnight cultures. These were grown at 37 ^{o}C until OD_{600} were about 0.8. To induce expression and heme biosynthesis, about 0.1 mM IPTG and 0.5mM 5-aminolevulinic acid hydrochloride (ALA) were added, respectively, to the cultures and incubations were continued overnight at 25 ^{o}C. A high concentration of ALA was used to increase the heme synthesis and heme protein production efficiency. The cells were harvested with centrifuge at 3000 xG, 10 ^{o}C for 15 minutes. Pelleted cells were stored at -80 ^{o}C for isolation and purification.

2.4.2. Protein extraction

Protein extraction and purification of all variants were done using the Gravity-Flow Column with HisPur Ni-NTA Resin using three buffers (buffers A, B and C) shown in the Table 2.4.

Table 2.4. Buffers for *Tt*H-NOX isolation and purification.

Buffers	Triethanolamine (mM)	Imidazole (mM)	Sodium Chloride (mM)	Benzamidine Hydrochloride (mM)	Phenylmethylsufonyl Fluoride (mM)
Lysis Buffer (Buffer A)	50	10	300	1.34	0.2
Elution Buffer (Buffer B)	50	150	300	-	-
Dialysis Buffer (Buffer C)	50	-	20 with 5 % glycerol	-	-

After determining the weight of the cell pellets, buffer A was added to the cells in a 1:1 (mass: volume) ratio. The dissolved cell lysates were sonicated on ice with an interval of 30 seconds for an average of 7 cycles until a watery consistency was achieved. Next, the lysates were heated for 40 minutes at 70 ^oC and pelleted at 3900 xG (10 ^oC) for 2 hours.

2.4.3. Protein purification through affinity chromatography

About 1 ml Nickel-NTA resin (Thermo Scientific) was prepared in column according to the protocol that was provided. The column with the settled resin was equilibrated with 3-5 ml of buffer A. The supernatants that were obtained after the centrifugation were added to the column. For this type of purification, the *Tt*H-NOX protein which has a C-terminal His-tag binds to the Ni-NTA resin. The low imidazole concentration in buffer A allows proteins with weak bindings through leaving the tighter bound ones in the column, selecting for better binding proteins. The Flow Through samples (containing weak binding proteins) were collected. The column was then washed with 25-30 volumes of buffer A until the wavelength at 280 nm was stable. Elution was performed with a high imidazole concentration buffer B in 1 ml aliquots.

Further purification to remove imidazole and undesired small compounds was done by dialysis for the first two variant purification- wild type and H102C using buffer C. The eluted fractions were pooled into a semi-permeable membrane (Spectra/Por Molecular Porous Membrane Tubing). This was then placed in 1 L buffer C which was changed twice at an interval of 2 hours. The purified proteins were concentrated in 10 ml

Microsep Advance Centrifugal concentration tubes until a volume of about 800 µl. 100 µl aliquots were prepared and stored at -80 ^{o}C. To confirm the efficiency of isolation and purification, SDS PAGE analyses were performed using 10 µl aliquot samples that were collected at every step of the isolation and purification processes.

2.5. Chemical and Structural Analysis

2.5.1. Ultraviolet-Visible (UV) spectroscopic analysis

In order to determine the UV spectroscopic characteristics of the *Tt*H-NOX variants, 20 X dilutions using buffer C were prepared and the absorbance measurements 650 nm – 250 nm were taken. This large range wavelength includes the α/β peaks for protein structure, the heme peak or Soret peak (a peak in the blue region of the visible spectrum and ranges around 400 nm) and the protein peak at 280 nm (A280). The unique characteristics of each *Tt*H-NOX variant were observed through their α/β and Soret peaks

2.5.2. Measurement of *Tt*H-NOX heme concentration

The heme concentrations of pure *Tt*H-NOX variants were calculated using the pyridine hemochromagen assay. An oxidation solution of 0.5 M sodium hydroxide, pyridine, ultrapure water and 0.1 M potassium ferricyanide was mixed in a 1:1 ratio to the *Tt*H-NOX protein in 50 mM phosphate buffer. The sample was then reduced with 0.5 M sodium dithionite solution. Spectroscopic measurements (500-600 nm) were taken to determine the reduced peak (scan with the highest peak). Using the table and graph provided by Barr and Feng, 2015, the extinction coefficients and concentrations of the *Tt*H-NOX variants were calculated using the Soret peak (the peak in the blue wavelength of the visible spectrum) and the Beer's concentration law. This peak ranged from 415 nm to 404 nm and was unique to each variant. According to the law, absorbance, A, is directly proportional to the concentration, C, extinction coefficient, Ɛ, and the path length, ꞁ (Thermo Scientific Tech Tip #6). Using this formula, the heme concentrations were measured thus:

$$\mathrm{C} = A/\mathcal{E}.\,l \qquad (1)$$

2.6. Catalytic Analysis

In order to study the chemical and enzymatic properties of wild type and mutant *Tt*H-NOXs, two catalytic reactions; catalase reactions with hydrogen peroxide and oxidation of 2,2'-azino-bis(3-ethylbenzthiazoline-6-sulfonic acid) (ABTS) were performed. In all protocols, protein, substrate, reagent concentrations and measurement analyses were obtained from literature.

2.6.1. Reaction of WT and mutant *Tt*H-NOXs with hydrogen peroxide (H_2O_2)

The study and comparisons of the peroxidase activities of the wild type and mutant proteins were achieved through the catalytic degradation of H_2O_2 according to the equation below:

$$2H_2O_2 \rightarrow 2\,H_2O + O_2 \qquad (2)$$

In order to optimize the reaction conditions, a solution of WT *Tt*H-NOX (5 µM) and H_2O_2 (0.1, 0.2 and 1 mM) in 50 mM potassium phosphate buffer (pH 7.0) were prepared. The absorbance at $OD_{250\text{-}650}$ were measured at time intervals; T=0, 1, 5, 10, 15, 20, 25, 30, 35, 40, 45, 50, 55, and 60 minutes. After absorbance against wavelength graph analysis at each time point for each H_2O_2 concentration, the optimal reaction conditions were found to be as follows:

a) A 50 mM potassium phosphate buffer, pH 7.0
b) A final heme concentration of 5 µM
c) A H_2O_2 concentrations of 0.1 mM
d) A "no protein" control assay where the protein is replaced with the elution buffer C (the buffer in which the H-NOX proteins are in).
e) Time intervals of 0, 1,0, 5, 10, 15, 20, 30, 40 and 60 minutes.

With these reaction conditions, the H_2O_2 assays were set up for the wild type, distal and proximal mutant *Tt*H-NOXs. About 20 µl aliquots of the reaction mixture at every time point were stored at – 80 ^{o}C for the hydrogen peroxide quantification using the Quantitative Peroxide Assay: Aqueous Compatible Formulation Kit (Pierce). The absorbance measurements of hydrogen peroxide in the solution were done on a plate reader at 595 nm. A standard curve was prepared by taking the quantitative measurements of several H_2O_2 dilutions; 0, 20, 40, 60 and 120 µM. According to the values obtained, a graph of absorbance against H_2O_2 concentration, a graph was formed. The standard curve was used to measure the concentration of H_2O_2 at each time point for both WT and control assays. The percentages of hydrogen peroxide loss were calculated to study the catalase activity of the WT.

This protocol was used to measure the catalase activity of the distal and proximal *Tt*H-NOX mutant proteins on H_2O_2. Their spectroscopic and catalytic differences were measured and compared.

2.6.2. Catalytic oxidation of 2,2'-azino-bis(3-ethylbenzthiazoline-6-sulfonic acid) (ABTS)

In the known peroxidase-catalyzed reaction, the one-electron oxidation of ABTS into the green radical cation, $ABTS^{•+}$ was chosen to further study the catalytic performance of the *Tt*H-NOX variants. Using ABTS as a substrate, H_2O_2 with the help of a peroxidase, catalyzes its oxidation to its radical cation which has a characteristic deep green color and an absorbance maximum of 734 nm as seen in the equation 3:

ABTS **$ABTS^{•+}$** (3)

ABTS stock solutions were made by dissolving approximately 13 mg in ultrapure water. Three control kinetic experiments were set up with WT *Tt*H-NOX (5 µM) according to Table 2.5.

Table 2.5. Control experiment set up for ABTS oxidation assay.

Control Experiments	H_2O_2 Concentration (mM)	ABTS Concentration (mM)	pH of 50 mM Potassium Phosphate Buffer
1	0.025, 0.1, 0.25, 0.5 and 1	1	7.5
2	1	0.05, 0.1, 0.25, 0.5 and 1	7.5
3	1	1	5.8, 6.8, 7.5 and 8.0
4 (No Protein)	1	1	7.5
5 (No H_2O_2)	-	1	7.5

Using the set up above, the product, ABTS radical cation, formation was measured at 734 nm every minute for 15 minutes. The conditions for the oxidation reaction was found to be as follows:

a) A 50 mM potassium phosphate buffer, pH 7.5
b) A final protein concentration of 5 μM
c) A H_2O_2 concentration of 1 mM
d) A ABTS concentration of 1 mM
e) A "no protein" control assay where the protein is replaced with the elution buffer C (the buffer in which the H-NOX proteins are in).
f) A "no ABTS" control assay with only H_2O_2 and protein.

The spectroscopic characteristics and kinetic parameters were measured for each mutant and comparisons were made with the wild type and negative controls.

CHAPTER 3

RESULTS AND DISCUSSION

3.1. Cloning of Wild Type and Mutant *Tt*-HNOX

3.1.1. Site-Directed Mutagenesis by PCR

The cloning of mutant *Tt*-HNOX proteins was achieved through site-directed mutagenesis by PCR using the *Tt*-HNOX wild type (WT) gene insert in the pET20b (3716 bp) expression vector. Using the forward and reverse primers for each variant, PCR reactions using the Q5 site-directed mutagenesis kit were performed to clone the wild type and mutant plasmids, as described in the Methods section.

3.1.2. Transformation into DH5α Competent Cells

After PCR, the Kinase, Lipase, Dpnl (KLD) reaction was performed on each variant. The PCR products were then transformed into competent DH5α cells through the heat-shock technique (refer to the Methods section for details). For each variant, 4 to 6 colonies from each variant were selected for plasmid purification experiments and sequence analyses.

3.1.3. Plasmid Purification and Sequence Analysis

Each of cloned plasmids were purified using the Macherey-Nagel Kit for DNA Purification and their concentrations were measured using the NanoDrop Spectrophotometer. Concentration of the purified plasmids are shown in Table 3.1. All variants were sent for sequencing at the BIYOMER sequencing facility in Izmir Institute of Technology. The mutations were confirmed using the GENEIOUS program for sequence analysis. Sample colonies with mutations were selected for protein expression tests. The amino acid sequences are shown in appendix A.

Table 3.1. Concentrations of purified wild type and mutant plasmids.

Samples	Wild Type (ng/ ml)	H102C (ng/ ml)	H102Y (ng/ ml)	Y140A (ng/ ml)	Y140H (ng/ ml)
A	190.20	77.20	81.3	99.33	86.29
B	142.40	109.90	119.5	86.21	93.43
C	-	59.40	137.7	75.63	100.1
D	-	125.70	99.0	83.32	124.7
E	-	124.80	-	-	99.3

3.1.4. Expression of WT and Variants of *Tt*H-NOX Proteins in *E. coli*

All variant plasmids were transformed into BL21 (DE3) competent *E. coli* cells for protein expression. Overnight cultures of four selected colonies (labelled A, B, C, D) were prepared and protein expression was induced using IPTG for an hour after which sample cells were collected. These were then analyzed for protein expression by SDS PAGE analysis. Glycerol stocks were prepared for the samples with *Tt*-HNOX expression.

3.1.4.1. Expression of WT *Tt*H-NOX

SDS-PAGE analysis showed protein expression for colony B after one-hour expression induction with IPTG as shown in Figure 3.1. Samples were taken before induction with IPTG (t_0) and 1 hour after induction (t_1).

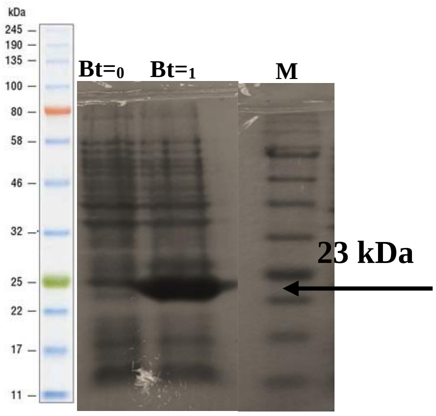

Figure 3.1 Protein expression band for WT *Tt*-HNOX (23,215 kDa). M: protein molecular weight marker. Colony t=$_0$ indicates control samples before IPTG induction whereas Colony t=$_1$ are samples after IPTG induction.

3.1.4.2. Expression of H102C variant *Tt*H-NOX

Out of four colonies tested (labeled A, B, C, D), SDS-PAGE Gel analysis showed positive protein expression for colony C after one-hour expression induction with IPTG (Figure 3.2). Glycerol stocks for colony C were prepared and stored at -80 ^{o}C.

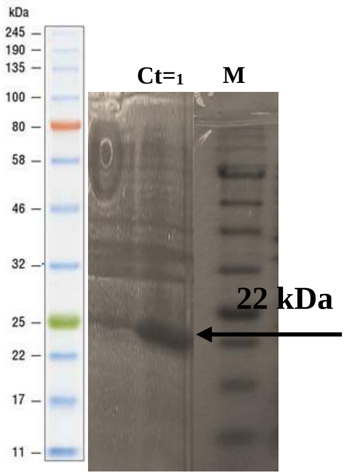

Figure 3.2 Protein expression band for *Tt*-HNOX H102C (21,882 kDa). M: protein molecular weight marker. Colony $t=_0$ indicates control sample before IPTG induction whereas Colony $t=_1$ is sample after IPTG induction.

3.1.4.3. Expression of H102Y variant *Tt*H-NOX

Out of four colonies tested (labeled A, B, C, D), SDS-PAGE Gel analysis showed positive protein expression for colonies A and B after one-hour expression induction with IPTG as seen in Figure 3.3. Glycerol stocks for colonies A and B were prepared and stored at -80 ^{o}C.

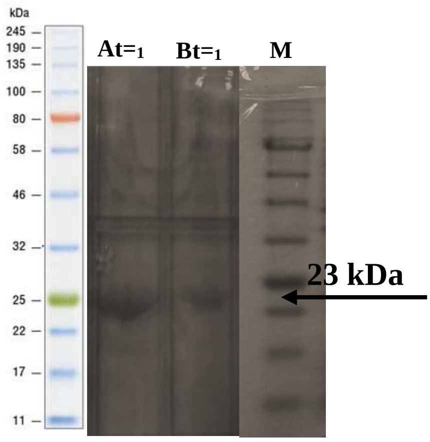

Figure 3.3 Protein expression band for *Tt*-HNOX H102Y (23,189 kDa). M: protein molecular weight marker. Colonies $t=_1$ are samples after IPTG induction.

3.1.4.4. Expression of Y140A variant *Tt*H-NOX

Out of four colonies tested (labeled A, B, C, D), SDS-PAGE Gel analysis showed positive protein expression for colonies C and D after one-hour expression induction with IPTG as seen in Figure 3.4. Glycerol stocks for colonies C and D were prepared and stored at -80 ^{o}C.

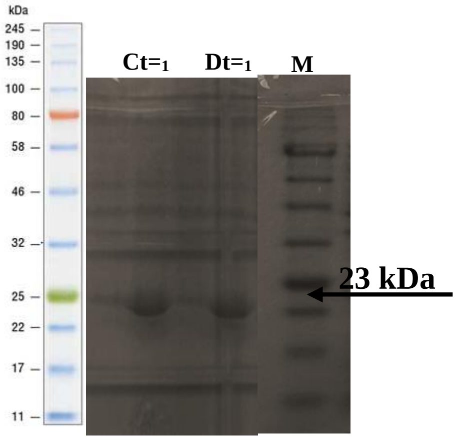

Figure 3.4 Protein expression band for *Tt*-HNOX Y140A (23,123 kDa). M: protein marker. Colonies $t=_{1}$ are samples after IPTG induction.

3.1.4.5. Expression of Y140H variant *Tt*H-NOX

Out of four colonies tested (labeled A, B, C, D), SDS-PAGE Gel analysis showed positive protein expression for colonies A and B after one-hour expression induction with IPTG (Figure 3.5). Glycerol stocks for colonies A and B were prepared and stored at -80 ^{o}C.

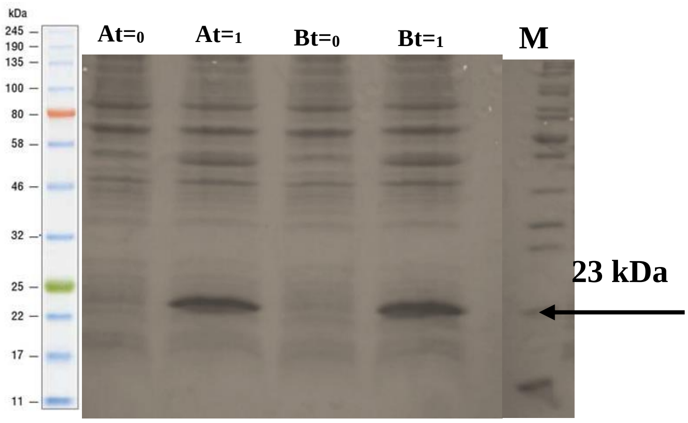

Figure 3.5 Protein expression band for *Tt*-HNOX Y140H (23,189 kDa). M: protein molecular weight marker. Colony $t=_{0}$ indicates control samples before IPTG induction whereas Colony $t=_{1}$ are samples after IPTG induction.

3.2. Extraction and Purification of WT and variants of *Tt*-HNOX Proteins

In order to isolate and purify the wild type and mutant *Tt*-HNOX proteins, protein expressions were induced on a large scale. The proteins were then isolated using the affinity chromatography method, the Gravity-flow Column with HisPur Ni-NTA Resin, as described in the Methods section. The isolation was followed by the removal of excess imidazole through desalting column or dialysis. Sample fractions from each extraction and purification step were collected for SDS PAGE analysis.

3.2.1. Pyridine Hemochromagen Assay

The heme content of WT and mutant *Tt*H-NOX hemeproteins were quantified using the pyridine hemochromagen method as described in section 2.5. Using their respective intense absorption peaks and the table provided by Barr and Guo, 2015, the concentrations and extinction coefficients of the *Tt*H-NOX variants were determined through the Beer's law. The extinction coefficients and yields are summarized in Table 3.2.

Table 3.2. Extinction coefficient and yield of purified WT and Mutant *Tt*H-NOXs

***Tt*H-NOX**	**Extinction Coefficient ($mM^{-1}cM^{-1}$)**	**Yield (mg)**
Wild Type	89	3.3
H102C	106.6	2.5
H102Y	128.1	6.2
Y140A	149.0	1.5
Y140H	125.7	0.9

3.2.2. Isolation and Purification of WT *Tt*H-NOX

About 12.3 g of cells were harvested after 1 L large scale expression as described in 2.4.1. section of the Methodology. After the final step in protein purification through dialysis, the final concentration of *Tt*H-NOX protein was determined to be 192 μM. The final yield of the protein was about 3.3 mg. SDS PAGE analysis of samples from each purification step is shown in Figure 3.6. Since no protein was observed in the third wash, no further washes were performed.

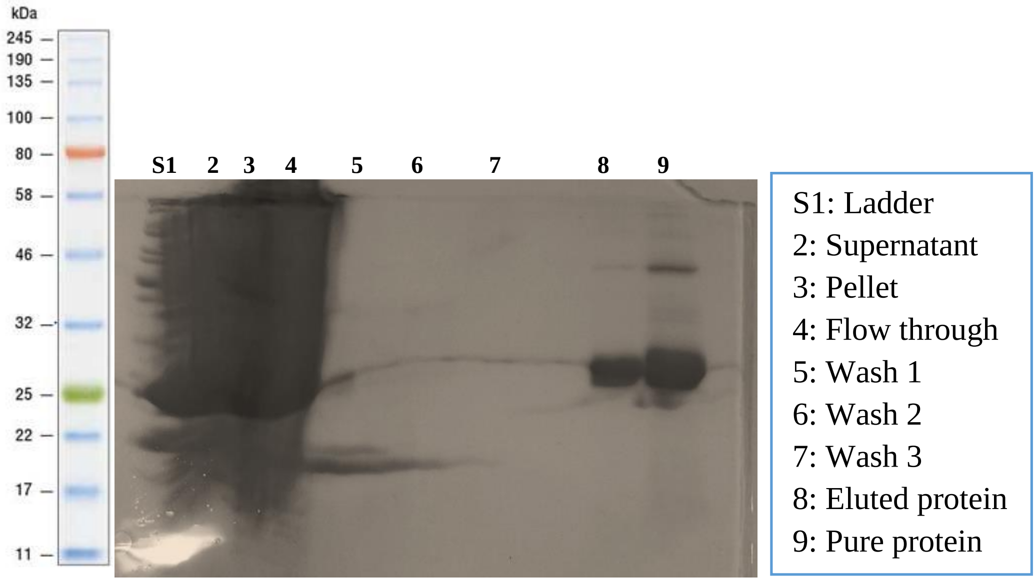

Figure 3.6 SDS-PAGE purification analysis for WT *Tt*H-NOX. The last two protein bands were about 23 kDa.

3.2.3. Isolation and purification of *Tt*H-NOX H102C

After 1 L protein expression, about 16.4 g of cells were harvested. The final concentration of *Tt*H-NOX H102C protein was 143 μM with a yield of 2.5 mg. SDS PAGE analysis of samples from each purification step is shown in Figure 3.7.

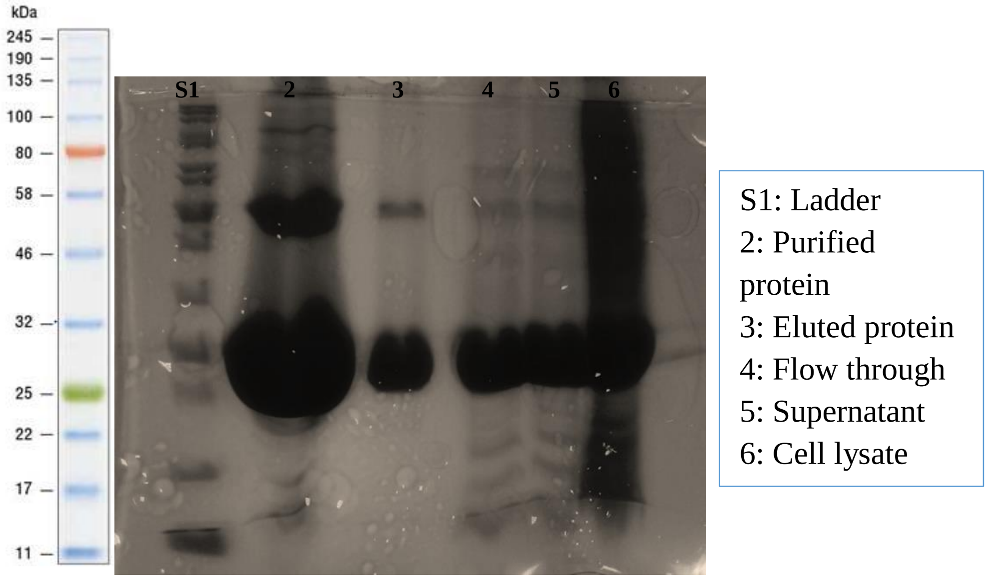

Figure 3.7. SDS-PAGE purification analysis for *Tt*H-NOX H102C.

3.2.4. Isolation and Purification of *Tt*H-NOX H102Y

After 1 L protein expression, about 13.130 g of cells were harvested. The final concentration and yield of *Tt*H-NOX H102Y protein were 149 μM and 6.2 mg respectively. SDS PAGE analysis of samples from each purification step is shown in Figure 3.8.

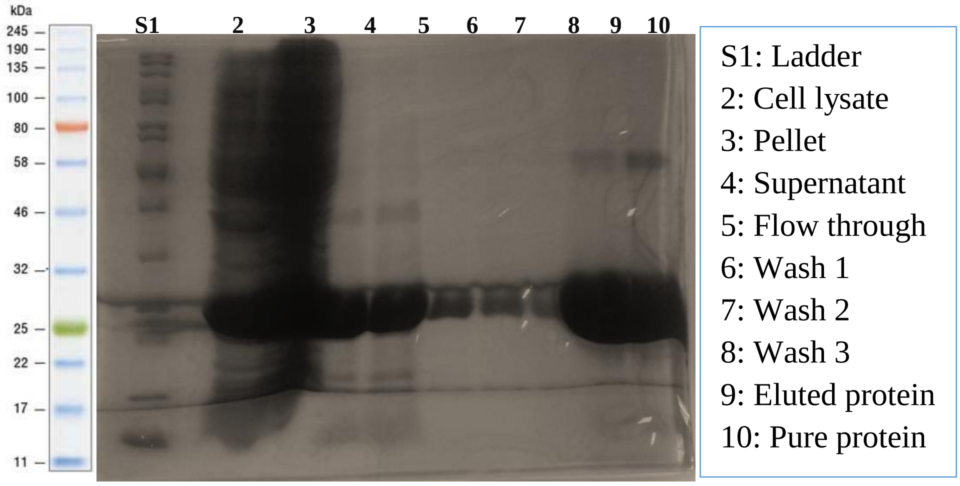

Figure 3.8. SDS-PAGE purification analysis for *Tt*H-NOX H102Y.

3.2.5. Isolation and purification of *Tt*H-NOX Y140A

After 1 L protein expression, about 16.7 g of cells were harvested. The final concentration of *Tt*H-NOX Y140A protein was 43 μM with a yield of 1.5 mg. SDS PAGE analysis of samples from each purification step is shown in Figure 3.9.

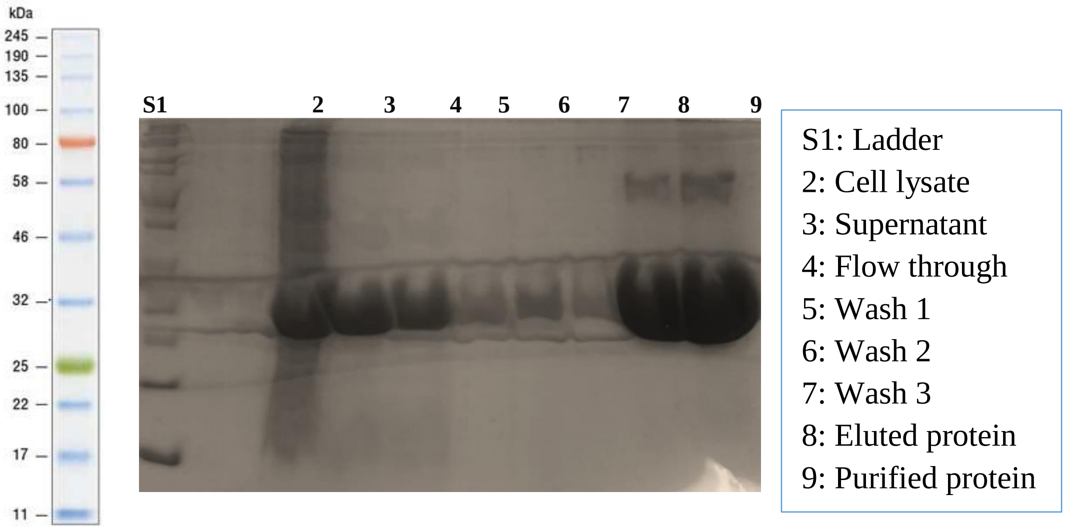

Figure 3.9. SDS-PAGE purification analysis for *Tt*H-NOX Y140A.

3.2.6. Isolation and purification of *Tt*H-NOX Y140H

After a 0.5 L protein expression, only about 3.8 g of *Tt*H-NOX Y140H BL21 (DE3) expressing cells were harvested. The final concentration and yield for the protein were 46 µM and 0.9 mg respectively. SDS PAGE analysis of samples from each purification step is shown in Figure 3.10.

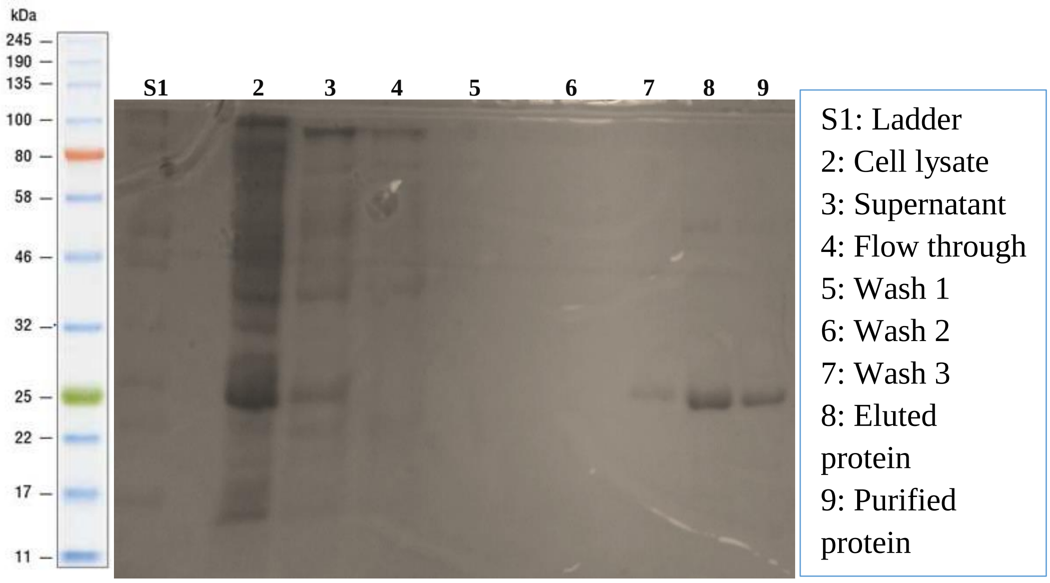

Figure 3.10. SDS-PAGE purification analysis for *Tt*H-NOX Y140H.

3.3. Spectrophotometric Analysis of Purified *Tt*H-NOX Proteins

To study the spectroscopic characteristics of the variant proteins, the absorbance measurements (A_{650} to A_{250}) of the 20 - 50 X diluted proteins in buffer C (please refer to section 2.4.2 of the Methodology) were taken. The measurements show the Soret peaks (an intense peak at the maximum wavelength for heme absorption), and the alpha/beta (α/β) bands. The Soret and α/β bands come from the heme, and absorbance at 280 nm due to tyrosine and tryptophan residues. UV-Vis spectroscopy results indicate high protein purity and correct protein folds. The results show intense Soret peaks shifts of the mutant from that of the wild type protein. The Soret peak for the wild type is the same as that found in literature for ferrous oxy-*Tt*H-NOX species. The recorded Soret and α/β peaks for WT *Tt*H-NOX is 415 nm and 590/550 nm respectively. All the mutant proteins showed intense Soret peak shifts from that of the wild type as seen in Table 3.3. Figure 3.11 shows the spectroscopic differences of the wild type and variant proteins.

Table 3.3. The UV spectral features of wild type *Tt*H-NOX and mutants.

***Tt*H-NOX**	**Soret (nm)**	**α/β Peaks (nm)**
WT	415	590/554
H102C	405	577/541
H102Y	404	556/509
Y140A	410	593/538
Y140H	409	576/546

The proximal mutants, H102Y and H102C, show intense shift in Soret peaks (Figure 3.12) suggesting a change in the proximal axial binding conformation of the ferrous iron at the active site. The H102Y mutant spectroscopic characteristics suggests a ligation of the phenol group to the iron whilst that of the H102C mutant suggests a thiolate-ligation to the heme forming a thiolate-bound five-coordinate state. These results show that both the tyrosine and cysteine residues replaced histidine at the proximal axial residue. In addition to the changes in the Soret band, changes in the α/β peaks indicate a significant change in the electronic structure in the heme iron. Furthermore, the mutants obtained have a larger 280 nm to Soret absorbance ratio indicating the presence of apoprotein (Figure 3.11), this is to be expected as residues surrounding the heme are mutated.

The Y140A and Y140H mutations have changed the accessibility and polarity of the distal pocket causing a shift in the Soret as seen in Figure 3.13. The replacement of the polar distal tyrosine residue to a less polar, small alanine residue for Y140A changed the polarity of the active site. The now less hindered active site might allow the introduction of water molecules which would interfere with the formation of stable complexes with oxygen and the electronic state of the heme. In the case of Y140H, the replacement of the neutral distal tyrosine with a positively charged histidine caused a change in the electronic charge of the distal pocket.

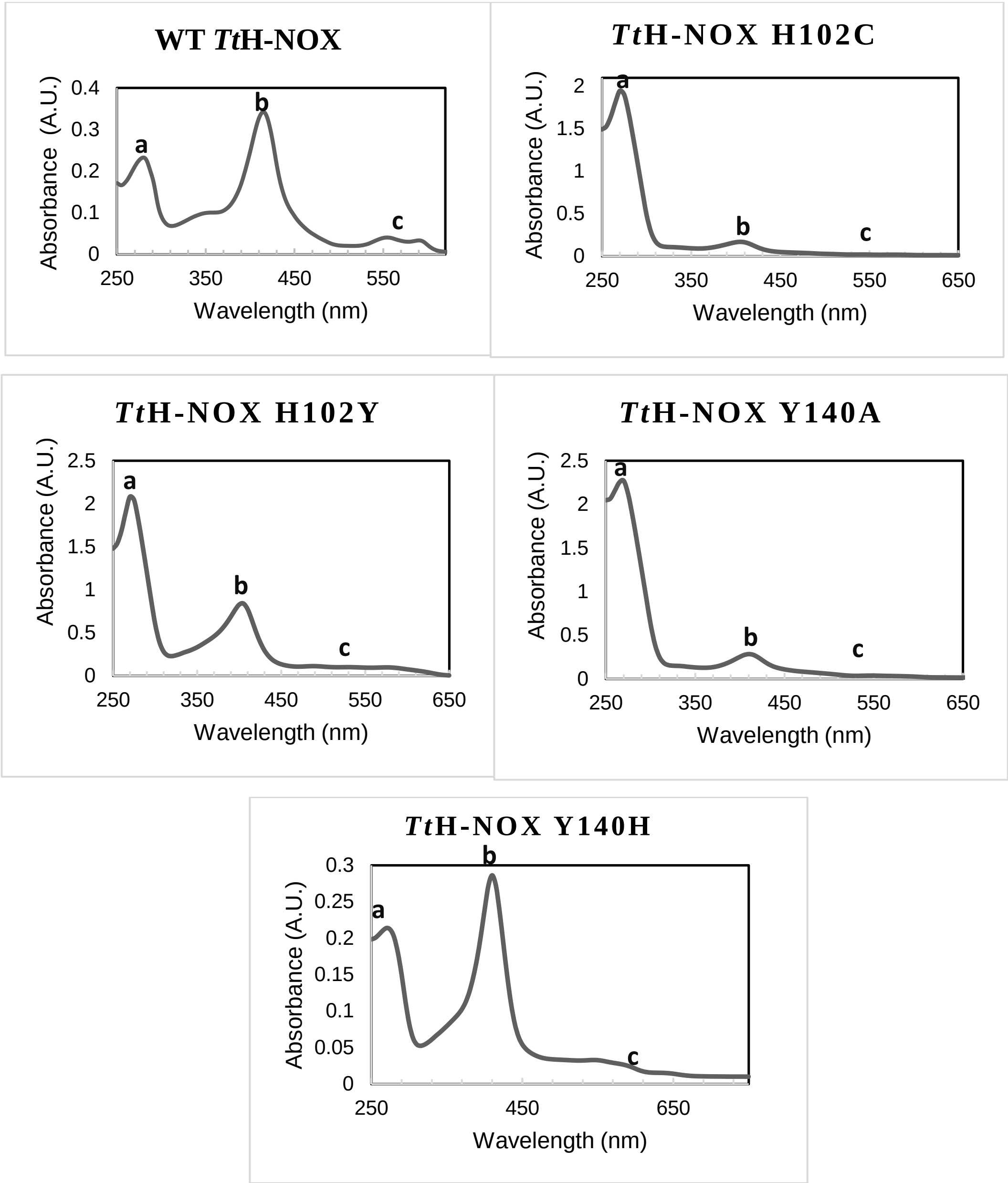

Figure 3.11 The UV-Vis spectra of the wild type and mutant of *Tt*H-NOX proteins. Labels a, b and c depict the absorbance at 280 nm, Soret peak and α/β peaks respectively. All the mutants show a deviation of Soret from that of the wild type.

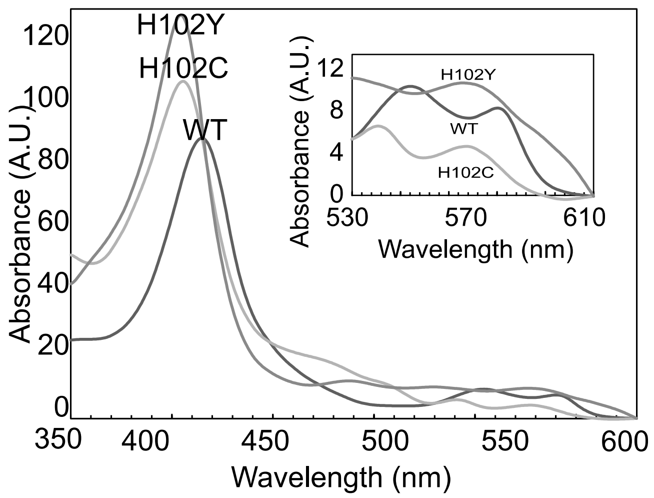

Figure 3.12 Spectral differences of wild type and mutant *Tt*H-NOX. The absorbance values were normalized at the Soret in order to fit the graph. Inset: focus on α/β peaks.

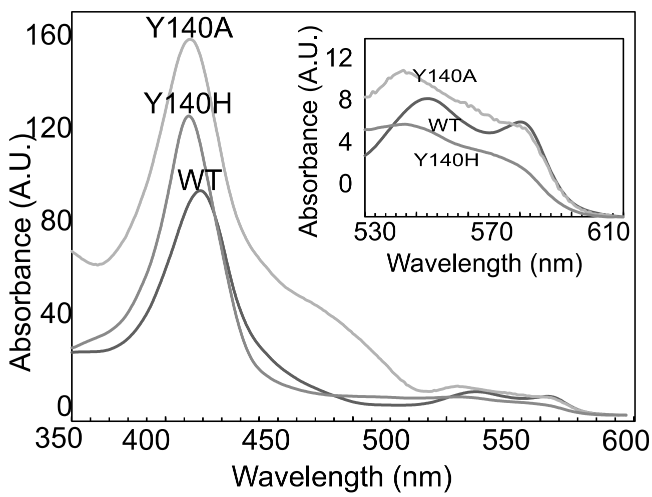

Figure 3.13 Spectral differences of wild type and mutant *Tt*H-NOXs. Absorbance values were normalized at the heme absorbance to fit the graph. Inset: focus on α/β peaks.

Each variant had different spectroscopic changes which are due to the changes in the heme active site structure. The spectral results also show that the changes in the proximal and distal pockets of the heme affected the electronic state of the heme iron (Fe) and the binding specificities. However, the effects were less significant for the distal residues because they are more distant from the heme Fe. In a previous study with *Tt*H-NOX where a tyrosine-140-leucine mutation was done, the mutant had a Soret peak of 422 nm with a reduced affinity for oxygen at the distal pocket (Boon and Marletta, 2005).

The tyrosine mutation in this study had Soret peaks of 409 nm, a deviation from the Soret in literature.

The cloning of *Tt*H-NOX by rational design was successful indicating that this heme protein is an ideal scaffold for rational design. Firstly, the *Tt*H-NOX protein is a thermophilic protein meaning that it does not require a temperature-controlled environment. It also has a characteristic red color making it easier for isolation and purification. In addition, all the mutations performed were successful and each protein variant had special spectroscopic characteristics. Finally, the process of cloning, isolation and purification did not affect the protein fold or significantly denature the protein.

3.4. Chemical Characterizations

3.4.1. Catalase Activity: Reaction with Hydrogen Peroxide (H_2O_2)

Catalases catalyze the decomposition of hydrogen peroxide to water and oxygen in two steps producing compounds I and II respectively (Boon et al., 2007). The ferriprotoporphyrin IX prosthetic group in the ferric state reacts with hydrogen peroxide to form the intermediate compound I. Compound 1 is then reduced to form the ferric enzyme through the intermediate compound II (Moffet et al., 2000).

$$\mathrm{Fe(III)} + H_2O_2 \longrightarrow \text{Compound I } (+5) \longrightarrow \text{Compound II } (+5) \longrightarrow \mathrm{Fe(III)} \quad (1)$$

It has been found that at a suitable distance to the heme Fe, the positioning of a distal histidine in a myoglobin scaffold enhanced the reduction of hydrogen peroxide. With this in mind, the WT and mutant *Tt*H-NOXs were tested for their catalase activities.

3.4.1.1. Spectroscopic changes of WT *Tt*H-NOX with H_2O_2 at room temperature

In order to test for the catalase activity of WT *Tt*H-NOX and its variants with H_2O_2, the reaction conditions were first optimized to obtain the best results for the assay. The control experiments were performed using the WT *Tt*H-NOX protein.

To determine the best conditions for the catalase assays, the WT *Tt*H-NOX was mixed with varying concentrations of hydrogen peroxide, 0.1, 0.2 and 1 mM. The reaction with 0.1 mM H_2O_2 and 10 µM WT protein (with respect to the holoprotein) in potassium phosphate buffer (pH 7.0) for 120 minutes showed the best results. These conditions were used for all the variants spectroscopic measurements. The "no protein" controls showed no changes in absorption spectra.

3.4.1.2. Reaction of WT *Tt*H-NOX with H_2O_2

In order to monitor the spectroscopic changes of the WT *Tt*H-NOX with H_2O_2, the absorbance values at 220-550 nm were measured at time points, T= 0, 5, 10, 20, 40, and 60 minutes at room temperature. Absorbance measurements, A_{350} to A_{550}, were followed at each time point (Figure 3.14). In addition, the concentration of H_2O_2 at various time points were quantified using a H_2O_2 quantitative kit as described in the methods section 2.6.1. These concentrations were compared with the "no protein" control assay. Difference spectra values were calculated to identify clear changes at the Soret. These were calculated by subtraction of the spectrum at each time point from the spectrum at time point zero.

The Soret absorbance of WT *Tt*H-NOX decreased with time. After 120 minutes, the decrease in heme was still in the linear range so, the reaction was allowed for go on for one more hour. The result shows a slow exponential decrease in the heme at 415 nm (Figure 3.14b).

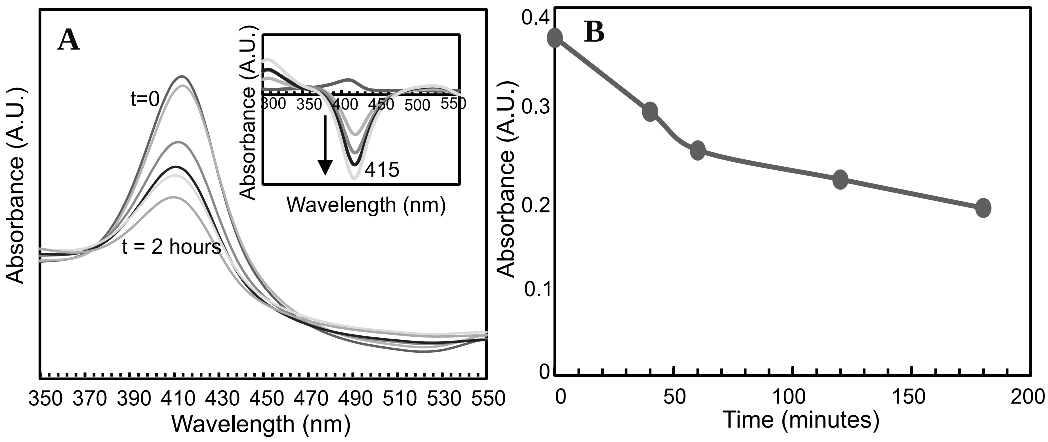

Figure 3.14 Absorption spectra of the catalase activity of WT *Tt*H-NOX. For this assay, 10 µM WT *Tt*H-NOX was mixed with 0.1 mM H_2O_2 in 50 mM phosphate buffer at pH 7.0. The graph shows a decrease in Soret over time. (B) The change in Soret over time. This shows a slow decrease during 120 minutes.

3.4.1.3. Reaction of *Tt*H-NOX H102C with H_2O_2

Under the same conditions as the WT *Tt*H-NOX experiments, the catalase activity for H102C variant of *Tt*H-NOX was measured as seen in Figure 3.16. In contrast to WT *Tt*H-NOX, the H102C mutant showed an increase in the Soret absorbance with time (Figure 3.15).

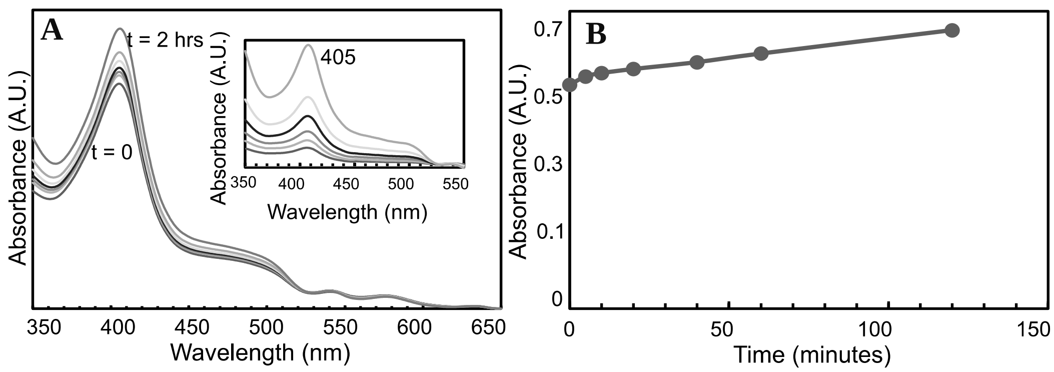

Figure 3.15 Absorption spectra of the catalase activity of the H102C mutant. This shows increases in Soret over time with new peaks. Insert: The difference spectra showing increase at the Soret peak. (B) Slight increase in Soret absorbance over time.

3.4.1.4. Reaction of *Tt*H-NOX H102Y with H_2O_2

During the reaction of the H102Y mutant and H_2O_2, the UV-visible spectra showed no significant changes (Figure 3.16). There were neither changes in the Soret nor changes in the absorbance values with time.

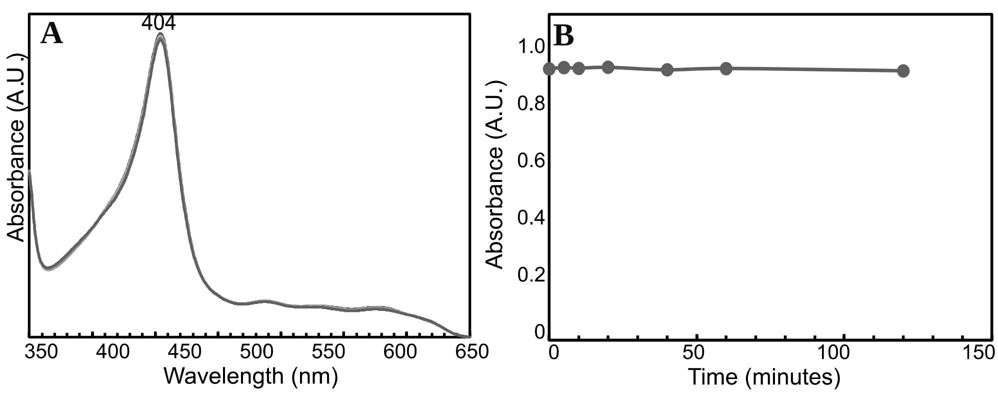

Figure 3.16 The Absorption spectra of the catalase activity of the H102Y mutant. (B) No significant changes in the Soret over time.

3.4.1.5. Reaction of *Tt*H-NOX Y140A with H_2O_2

During the reaction of the Y140A mutant with H_2O_2, there were increases in the absorbance values over time. In addition, there was a significant shift in the Soret with time from the starting Soret maximum absorbance at 409 nm. Over 120 minutes, the Soret gradually shifted to 405 nm (Figure 3.17).

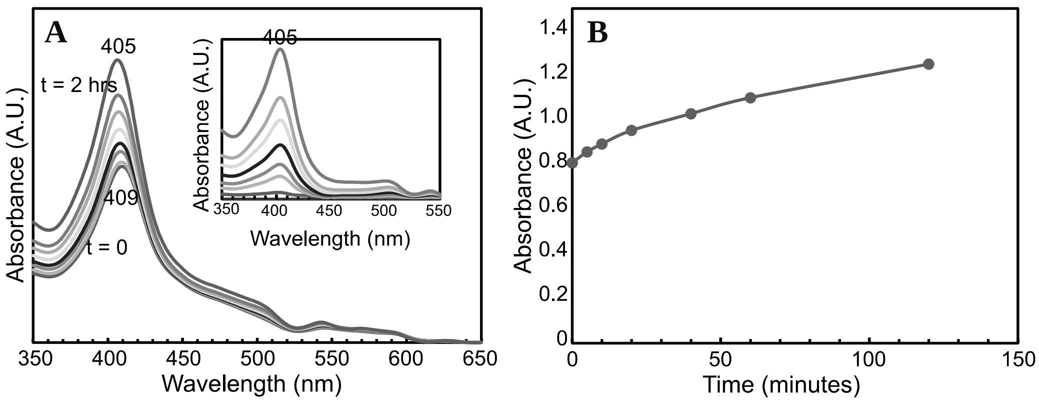

Figure 3.17 Absorption spectra of the catalase activity of the Y140A mutant. This shows the gradual shifts in the Soret peak with time. Insert: The difference spectra showing the gradual shift and increases at the Soret peak. (B) The increases in the Soret with time.

3.4.1.6. Reaction of *Tt*H-NOX Y140H with H_2O_2

The Y140H mutant exhibited a different reactivity with H_2O_2 when compared to the other variants and WT *Tt*H-NOX. Not only were there increases in the absorption over time, there was also a rapid shift of the Soret maximum absorbance from 409 nm to 415 nm initially, and then the Soret shifted back to 409 nm (Figure 3.18). This shift is thought to be due to the formation of the intermediate compound II before the oxidation of hydrogen peroxide is completed. In order to significantly change the reaction time, the reaction was repeated at 8 ^{o}C. As seen in Figure 3.18, the Soret also shifted to 415 nm under 2 minutes. The absorbance at 409 nm also showed an increase for the first 10 minutes followed by a decrease in the following 20 minutes.

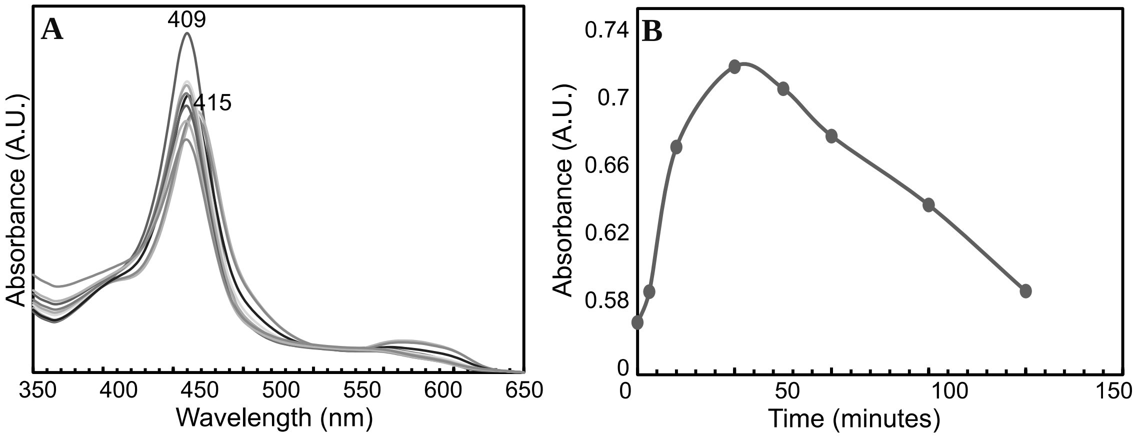

Figure 3.18 The absorbance changes for the reaction between Y140H *Tt*H-NOX and H_2O_2. The shift in the Soret during the first two minutes of the reaction, an increase in Soret for the next 10 minutes and a decrease after 10 minutes can be observed. (B) The absorbance changes at 409 nm for the Y140H mutant. This shows an increase followed by a decrease in absorbance of the Soret over time.

3.4.2. Quantitative analysis of reduced H_2O_2

All five variants showed different spectroscopic changes in response to their reactions with hydrogen peroxide. In order to measure the catalytic efficiency of each variant, samples were collected and unreacted H_2O_2 was quantified at each time point using the Quantitative Peroxide Assay Kits (as described in the Methods section). The amount of H_2O_2 consumed was determined by subtracting this amount from the hydrogen peroxide at the beginning of the reaction. The concentrations of hydrogen peroxide in the assays were determined through standard curves which were prepared for each experiment. The percentage loss of hydrogen peroxide for each *Tt*H-NOX variant was calculated and their differences are shown in Table 3.4.

Table 3.4. The percentage loss of hydrogen peroxide at 1 minute and after 120 minutes in the presence and absence of WT *Tt*H-NOX and its variants.

***Tt*H-NOX**	**Percentage Loss of H_2O_2 at 1 Minute (%)**	**“No Protein” Control at 1 Minute(%)**	**Percentage Loss of H_2O_2 at 120 Minutes(%)**	**“No Protein” Control (%)**
WT	36 ± 0.6	2.4 ± 1.6	93 ± 1.2	28 ± 9.0
H102C	5 ± 0.9	1.2 ± 0.5	52 ± 0.6	8 ± 2.0
H102Y	11 ± 6.0	9.7 ± 1.1	81 ± 2.1	10 ± 1.3
Y140A	3 ± 1.7	3.9 ± 2.7	56 ±2.3	10 ± 1.8
Y140H	90 ± 0.3	0.7 ± 0.3	97 ± 0.9	11 ± 7.1

As seen in Figure 3.24, the WT *Tt*H-NOX protein catalyzed the decomposition of hydrogen peroxide by 93 percent in 2 hours. In comparison, the “no protein” control showed no significant change nor decay of the hydrogen peroxide. This suggests that the WT *Tt*H-NOX can act as a catalase enzyme which can catalyze H_2O_2 decomposition under mild reaction conditions.

The H102C mutant catalyzed about 52 percent of the hydrogen peroxide decomposition indicating that this mutant has a lower catalytic efficiency than the wild type. However, the creation of new peaks suggests that there might be two independent reactions which can be tested by an oxidation experiment with ferrocyanide. The H102Y mutant showed no change in its spectroscopic characteristics but, it catalyzed about 81 percent of the hydrogen peroxide. Although it is lower than that of the wild type, this difference suggests that the mutant is highly stable.

The distal mutants show shifts in the Soret maximum absorbance over the course of the reactions. The Y140A mutant which exhibited a gradual Soret shift converted 67 percent hydrogen peroxide. The Y140H mutant proved to be the best catalase for the decomposition of hydrogen peroxide (Figure 3.19). Y140H *Tt*H-NOX converted more than 97 percent of hydrogen peroxide in less than two minutes. During this time, there was an intense shift in Soret to 415 nm and back to 409 nm. This can be due to the formation of the 6-coordinate compound II intermediate of the heme.

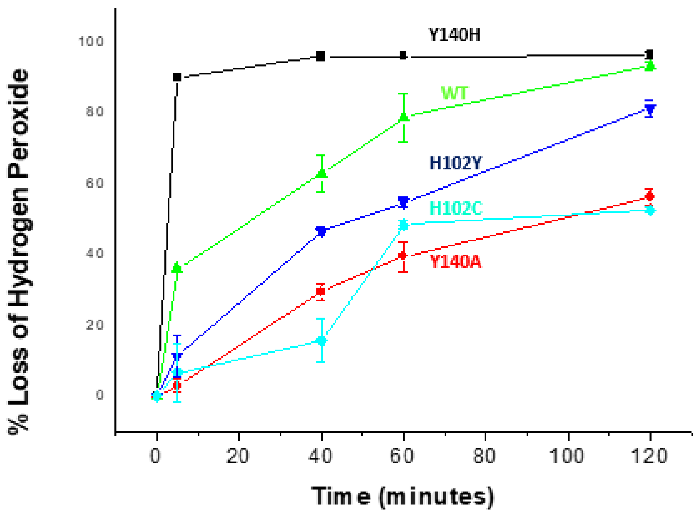

Figure 3.19 The percentage loss of hydrogen peroxide by each *Tt*H-NOX variant. Only the Y140H mutant exhibited a higher peroxidase activity that the wild type.

All the variant proteins exhibited differences in their catalase activities. Even though the WT *Tt*H-NOX showed catalase activity as compared to the negative control, the Y140H mutant showed a much higher catalase activity. The catalase activity for Y140H *Tt*H-NOX was the most efficient (with an intermediate compound II formation) as the entire reaction completed in under 2 minutes making this mutant the best catalase. The H102C mutant showed the lowest catalysis, catalyzing only 52 % of the reaction, and showed the most spectroscopic changes. Though H102Y mutant was able to catalyze the reaction to some extent, it did not show any significant changes in its spectroscopic features. This observation suggests that the mutant is highly stable. Finally, the distal mutant, Y140A, had a special characteristic where the Soret gradually shifted to 409 nm at the start to 405 nm at the end of the reaction. This suggests a change in the polarity of the distal heme environment.

3.4.3. Oxidation of 2, 2'-azino-bis(3-ethylbenzthiazoline-6-sulfonic acid) (ABTS)

Peroxidases are enzymes that catalyze the reduction of hydrogen peroxide to form water or the oxidation of a substrates (like ABTS or guaiacol) to radical cation and tetraguaiacol (Guo et al., 2012). To characterize and compare the peroxidase activity of the WT *Tt*H-NOX and its variants, the one-electron oxidation reactions of ABTS into the green radical cation, $ABTS^{\bullet+}$, were performed (Equation 1).

$$\textbf{ABTS} \xrightarrow[\textbf{\textit{Tt}H-NOX,}\ \mathbf{H_2O_2}]{} \mathbf{ABTS^{\bullet+}} + \boldsymbol{e^-} \qquad (1)$$

3.4.3.1. Catalytic activity of wild type *Tt*H-NOX with ABTS

The WT *Tt*H-NOX and H_2O_2 oxidized ABTS in aqueous solution. However, since the catalysis of ABTS oxidation has never been tested before on *Tt*H-NOX proteins, three different kinetic experiments had to be used to study their kinetics of reaction. These experiments investigated the oxidation of ABTS catalyzed by WT *Tt*H-NOX under varying concentrations of ABTS, H_2O_2 and at different pHs. In each experiment, the formation of the deep green $ABTS^{\bullet+}$ was followed by increase in absorbance at 734 nm, the maximum absorption of the $ABTS^{\bullet+}$ radical cation. The concentration of wild type protein used for each experiment was 5 µM and the absorbance measurements for the kinetic experiments were taken every minute for 15 minutes.

Figure 3.20 shows the first kinetic experiments using different ABTS concentrations of 0.05, 0.1, 0.25, 0.5 and 1 mM in the presence of 1 mM H_2O_2. This resulted in a sigmoidal kinetics in $ABTS^{\bullet +}$ formation with the highest activity observed for the assay of 1 mM ABTS. The assay with the 0.05 mM ABTS was much more sigmoidal than that with 1 mM ABTS. All sigmoidal reaction curves were confirmed after the derivative of increase in absorbance at each time point was calculated as seen in Figure 3.20b.

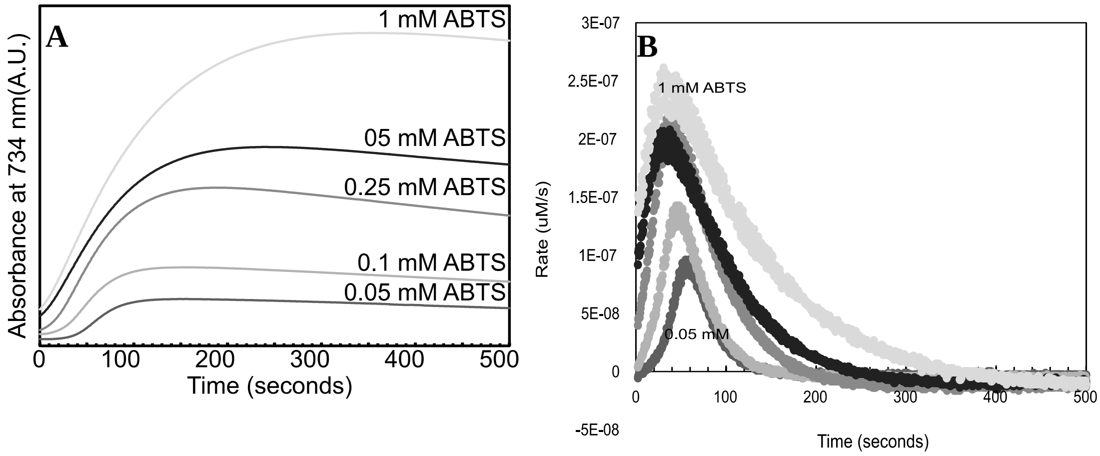

Figure 3.20 Reaction profiles of WT *Tt*H-NOX at 734 nm with different ABTS concentrations (A). Slope of Increase in 734 nm (B). The reactions were performed at 25 ^oC between 5 µM WT *Tt*H-NOX and 1 mM H_2O_2 at pH 7.5.

The second set of experiments were performed using different H_2O_2 concentrations of 0 (control), 0.025, 0.1, 0.25, 0.5 and 1 mM in the presence of 1 mM ABTS and 5 µM wild type *Tt*H-NOX at pH 7.5 for 15 minutes. The increase in absorbance was sigmoidal with the highest reaction rate observed at 1 mM H_2O_2 as seen in Figure 3.21. The "no H_2O_2" control had no measurable catalytic activity proving that the wild type enzyme only catalyzes the oxidation reaction in the presence H_2O_2. Again, the assay with the highest H_2O_2 concentration showed the highest activity with a less sigmoidal curve.

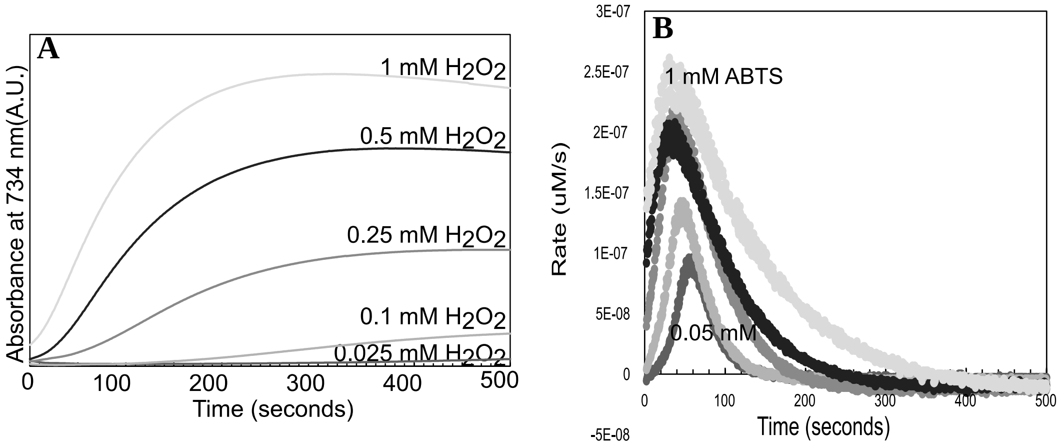

Figure 3.21 Reaction profiles of WT *Tt*H-NOX at 734 nm with different H_2O_2 concentrations (A). Slope of Increase in 734 nm (B). These were performed at 25°C between 5 µM WT *Tt*H-NOX and 1 mM ABTS at pH 7.5.

Finally, the last set of kinetic experiments were carried out in different pH ranges at 5.8, 6.8, 7.5 and 8.0 with 1 mM ABTS and 1 mM H_2O_2. The reaction at pH 5.8 exhibited a "near linear" exponential reaction curve whilst the other three pH ranges had the same sigmoidal characteristics as the two experiments described above (Figure 3.22). At pH 5.8, the reaction rate was highest with a less sigmoidal curve indicating that at that pH, the reaction was close to a classical enzyme reaction, an exponential-second order kinetics.

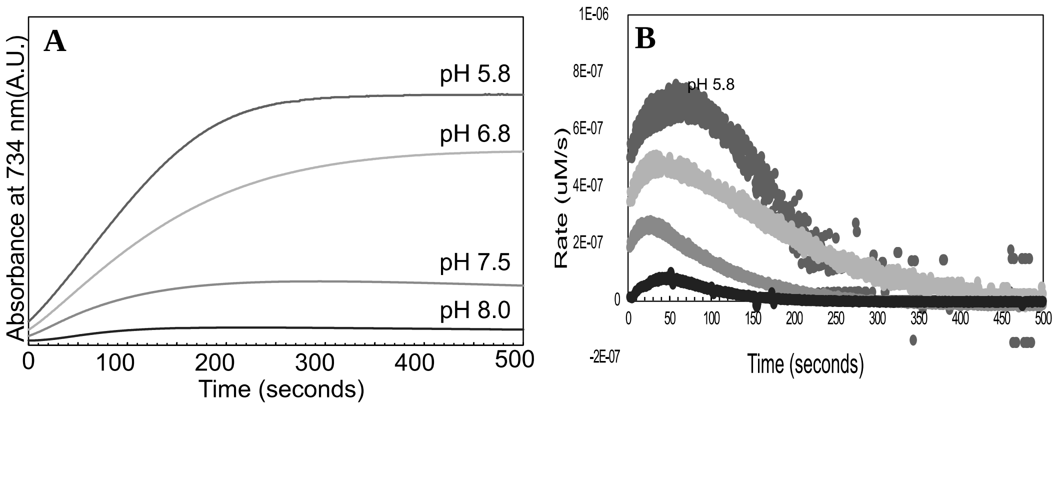

Figure 3.22 Reaction profiles of WT *Tt*H-NOX at 734 nm at different pHs (A). Slope of Increase in 734 nm (B). Even though the curves for pHs 5.8 and 6.8 were close to exponential, they still showed a slight sigmoidal effect at the very beginning of the assays.

The three kinetic studies for the wild type were all performed in duplicates and the analyses showed an enzyme efficiency with a pH and concentration dependence. They also showed a non-classical enzyme curve which slightly changes with varying substrate concentrations and pHs. These results prove that whilst *Tt*H-NOX can efficiently oxidize ABTS in the presence of H_2O_2, it does so in a non-classical enzyme kinetics way. This is also a deviation from the classical Michaelis-Menten curve.

3.4.3.2. Catalytic activity of WT *Tt*H-NOX towards ABTS oxidation

Figure 3.23 shows the full spectrum for the WT *Tt*H-NOX taken at each time point. As seen in the figure, the reaction was completed by 4 minutes and the $ABTS^{•+}$ formation absorbance values were observed to increase with time (Figure 3.23a). The rate of formation of the $ABTS^{•+}$ was also followed as seen in Figure 3.23b.

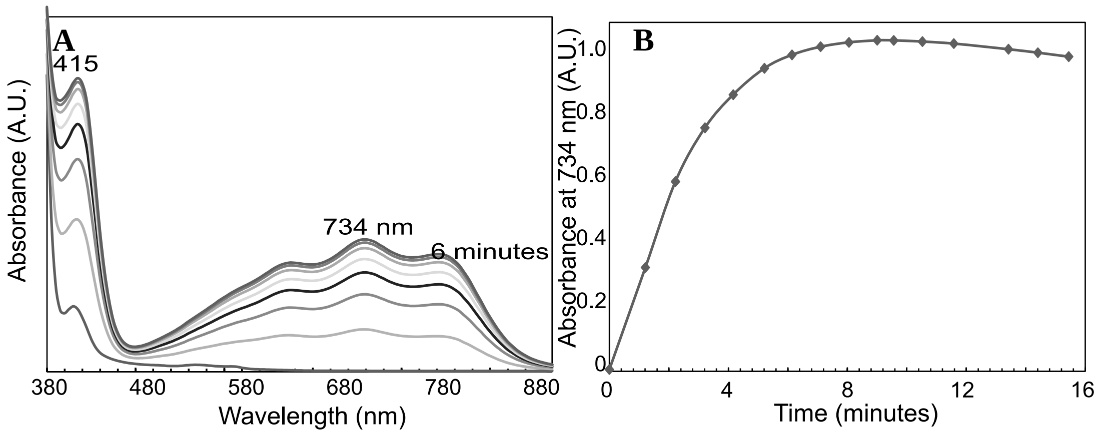

Figure 3.23 (A) The Spectroscopic and kinetic characteristics of WT *Tt*H-NOX. (B) $ABTS^{•+}$ formation at 734 nm with time.

3.4.3.3. Catalytic activity of *Tt*H-NOX mutants towards ABTS oxidation

As illustrated in Figure 3.24, the *Tt*H-NOX H102C mutant showed different spectra from that of the WT *Tt*H-NOX. Not only were there just slight increases in the Soret absorption over time, there were also no significant increases in the $ABTS^{•+}$ absorption even after one hour. This indicated that the mutant is very slow at catalyzing the oxidation of ABTS.

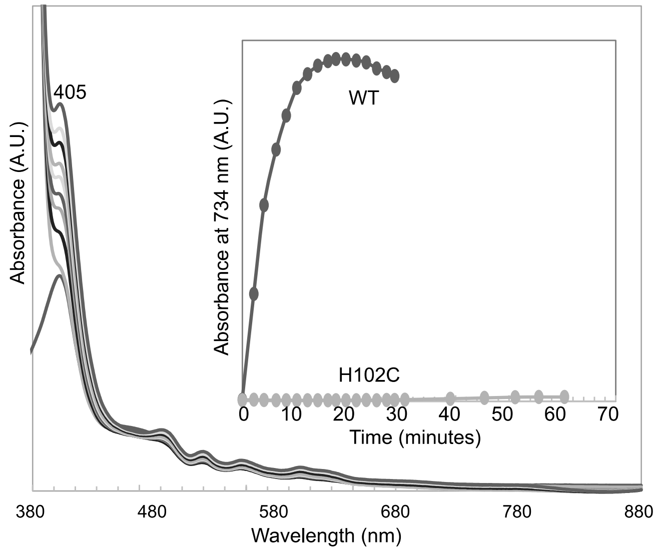

Figure 3.24 The Spectroscopic and kinetic characteristics of *Tt*H-NOX H102C. Inset: ABTS$^{\bullet+}$ formation by H102C as compared to WT.

The *Tt*H-NOX H102Y mutant did not catalyze the oxidation reaction as no changes in the Soret nor ABTS$^{\bullet+}$ formation with time was recorded. The assay was then repeated at a very low ABTS concentration of 30 µM for two hours in order to check for any decrease in ABTS concentration. As seen in Figure 3.25, the substrate, ABTS was still detectable at its absorbance maximum of 340 nm showing that this mutant did not catalyze the reaction at all.

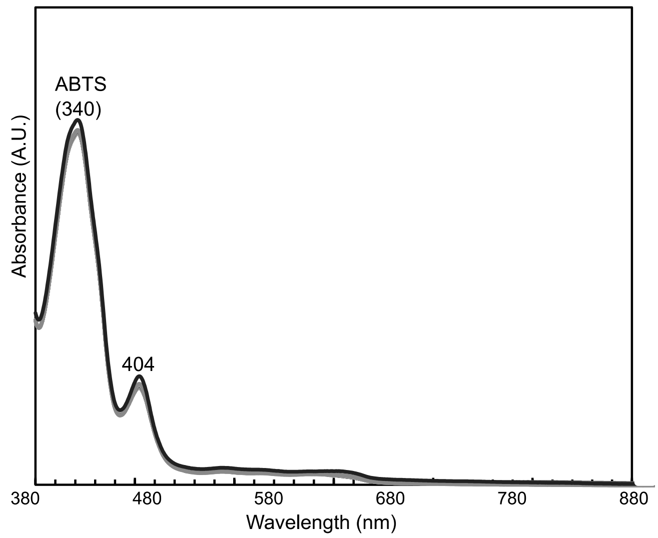

Figure 3.25 The Spectroscopic of *Tt*H-NOX H102Y. The Absorbance$_{maximum}$ of ABTS at 340 nm shows that this mutant did not catalyze the oxidation reaction.

The *Tt*H-NOX Y140A mutant exhibited slight increases in the $ABTS^{\bullet+}$ formation with time. However, the increases were insignificant and were observed after 30 minutes. The Soret at 409 nm did show increases with time as seen in Figure 3.26.

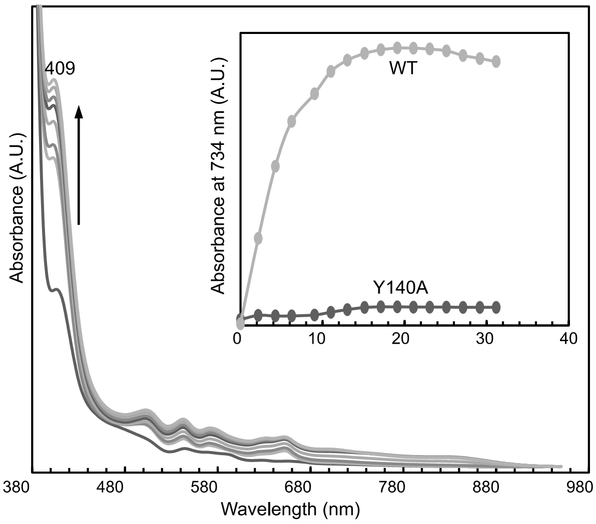

Figure 3.26 The Spectroscopic and kinetic characteristics of *Tt*H-NOX Y140A. Insert: $ABTS^{\bullet+}$ formation by Y140A as compared to WT.

Finally, the Y140H *Tt*H-NOX mutant catalyzed the oxidation reaction in the presence of H_2O_2 within seconds. The amount of the $ABTS^{\bullet+}$ sharply increased for a few seconds and then decreased for the next 5 minutes. Therefore, the result indicates that the reaction was completed in a few seconds. Figure 3.27 shows the product formation at 734 nm.

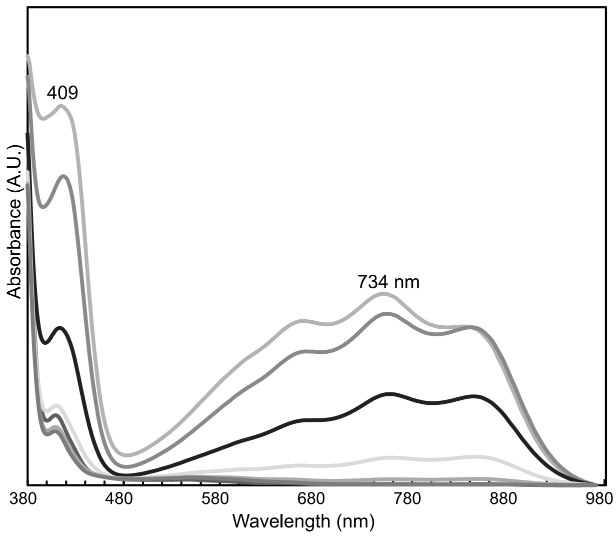

Figure 3.27 The Spectroscopic and kinetic characteristics of *Tt*H-NOX Y140H. There is an increase in the $ABTS^{\bullet+}$ absorbance for the first 2 minutes and decreases after the reaction completion.

To follow the formation of the $ABTS^{•+}$ more clearly with time, the reaction was repeated with 1 µM Y140H mutant and WT *Tt*H-NOX for comparison. The formation by Y140H exhibited an almost canonical oxidation kinetics as compared to the WT which was more sigmoidal. In addition, the assay with the Y140H mutant showed an approximately 5-fold increase in the rate than that of the WT. This result, as seen in Figure 3.28, shows that the Y140H *Tt*H-NOX catalyzes the oxidation of ABTS in the presence of H_2O_2 more efficiently that the wild type.

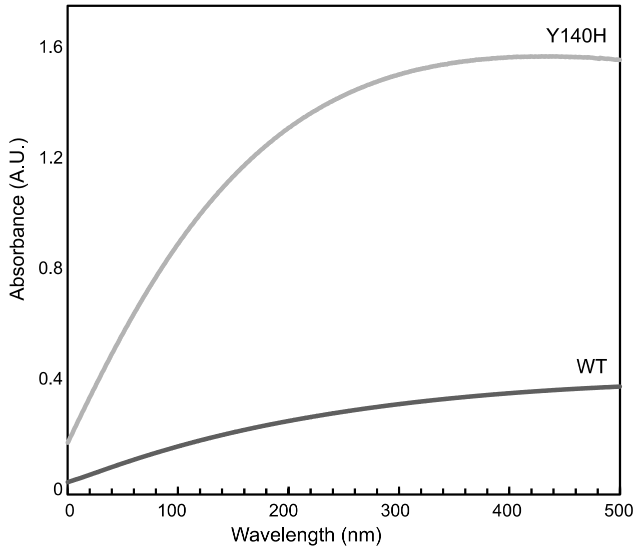

Figure 3.28 The oxidation kinetics for WT and Y140H *Tt*H-NOX. The Y140H mutant has an almost Michaelis-Menten kinetics and a 5-fold increase in $ABTS^{•+}$ formation as compared to the wild type.

3.4.3.4. Kinetic Parameters for the ABTS Oxidation Reaction

In order to determine the rate constant, turnover number and order of reaction for WT *Tt*H-NOX, the initial rate was determined at different ABTS concentrations (0.1, 0.25, 0.5, 0.8 and 1.0 µM) in the presence of 1.5 mM H_2O_2 with 5 µM WT *Tt*H-NOX (Figure 3.29). The second order rate constant and turnover number were determined to be 0.74 μMs^{-1} and 0.15 s^{-1}.

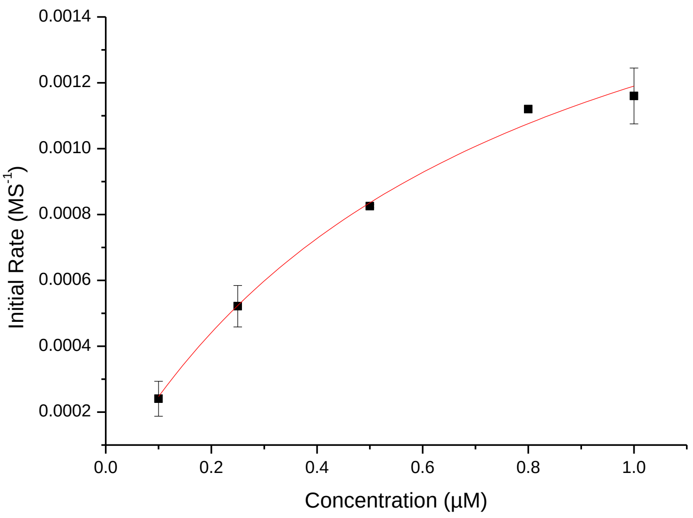

Figure 3.29 Kinetic parameters for ABTS oxidation using WT *Tt*H-NOX. The oxidation reaction has a second order rate constant of 0.74 μMs^{-1}.

Since this catalytic test has never been attempted on *Tt*H-NOX, the kinetic and spectroscopic experiments were important in studying the catalytic properties of the *Tt*H-NOX variants. First and foremost, the wild type catalyzed the reactions in a non-classical enzyme fashion. A classical enzyme curve is a typical Michaelis-Menten curve with a very short pre-steady state, an exponential increase in reaction velocity and a stationary phase. The wild type exhibited a deviation from this as it exhibited a sigmoidal type enzyme curve (Figures 3.25, 3.26 and 3.27). This can be explained as the wild type enzyme having a longer pre-steady state of catalysis meaning that there is a slow binding of the substrate (ABTS) to the WT *Tt*H-NOX.

In addition, the oxidation reaction of ABTS with WT *Tt*H-NOX had the highest reaction rate at pH 5.8. This result is similar to what was observed with myoglobin where the ABTS oxidation was highest at pH 5.8 (Carlsen and Vance, 2003). This study explained that the effect was due to the protonation of imidazole resulting in the opening of the heme Fe center for hydrogen bonding. Also, that the electrostatic binding of the ABTS anion to the protonated myoglobin facilitated electron transfer to compound II. Therefore, at pH 5.8, the heme center is protonated and leading to better substrate binding and higher reactivity. The same explanation can be given to what was observed in the WT *Tt*H-NOX where the low pH environment resulted in a protonation at the heme center causing a facilitated binding of the ABTS.

The proximal mutant *Tt*H-NOX H102C, catalyzed the reaction much more slowly than the wild type. Although there were increases the Soret absorption, the rate of reaction was too slow to allow accurate kinetic analyses. The *Tt*H-NOX H102Y mutant showed no reactivity with ABTS even at a very low ABTS concentration and no changes in Soret suggesting that it did not catalyze the oxidation reaction.

The distal mutants, Y140A and Y140H, exhibited different spectroscopic and kinetic characteristics for the oxidation of ABTS in the presence of hydrogen peroxide. Whilst, Y140A exhibited and insignificant increase in the formation of $ABTS^{\bullet+}$, the Y140H mutant catalyzed the reaction under 2 minutes and had a 5-fold increase in $ABTS^{\bullet+}$ as compared to the wild type. Also, Y140H mutant showed an almost second order kinetics for the oxidation reaction making it the most efficient *Tt*H-NOX variant for the oxidation of ABTS in the presence of hydrogen peroxide.

These results prove that the wild type is capable of oxidizing ABTS into its radical cation in an inefficient and non-canonical manner. Changes at the proximal pocket and the distal tyrosine to alanine significantly decreases its reaction with ABTS. However, changing the distal tyrosine to histidine increases its catalytic efficiency by 5-fold. Therefore, with this study the ABTS oxidation catalytic profile for WT *Tt*H-NOX has been established.

CHAPTER 4

CONCLUSION

Advances in protein engineering lead to efficient rational design strategies by site-directed mutagenesis. Rational design of proteins also provides a better understanding of the molecular mechanisms of enzymes. The engineering of enzymes by rational design through molecular assembly has not only created new and improved biocatalysts, but these biocatalysts can also synthesize enantiopure products that are environmentally friendly. Heme proteins are involved in diverse biological processes including catalysis of important biosynthetic reactions, making them good candidates for biocatalysis. In this study, the heme protein *Tt*H-NOX was re-shaped through rational design to create a novel thermophilic biocatalyst, to provide a better understanding on their molecular mechanisms and to aid in the design of future biocatalysts.

The successful cloning of the wild type and mutant *Tt*H-NOXs created new *Tt*H-NOX variants with spectroscopic and catalytic differences. The wild type showed similar results in the Soret of 415 nm as previously observed in literature. It also possessed a high peroxidase activity observed for the first time in literature, it oxidized the substrate, ABTS, efficiently. These observations prove that wild type *Tt*H-NOX is a good peroxidase and can be utilized as a peroxidase enzyme. The proximal mutations, *Tt*H-NOX H102C and *Tt*H-NOX H102Y, showed Soret peaks of 405 nm and 404 nm respectively. These variants also catalyzed the decomposition of hydrogen peroxide to some extent although they did so inefficiently. In addition, the two mutants were worse catalysts for the oxidation of ABTS. These results show the change in the proximal heme Fe ligand reduced the protein's catalytic reactivity by changing its molecular mechanism at the active site. The phenol and thiolate group ligations to the ferric heme led to difficulty in the dissociation of the new residues upon substrate binding thereby, reducing its reactivity and changing its enzymatic functions. The distal mutation, *Tt*H-NOX Y140A, also reduced the hydrogen peroxide but at a low rate when compared to the wild type. It also exhibited unique spectral characteristics where the Soret peak changed gradually during the reaction period. This might be due to the fact that the active site is much more open to other molecules (such as water) thereby changing the polarity of the active site and accessibility of the substrate to the heme Fe. On the other hand, the *Tt*H-NOX Y140H mutant exhibited an efficient peroxidase and catalase activities suggesting that it might be a new biocatalyst. This mutant decomposed hydrogen peroxide and oxidized ABTS at the fastest rate. This confirms that the presence of a distal histidine close to the heme increases the reactivity of the heme.

The signaling protein, *Tt*H-NOX can catalyze hydrogen peroxide decomposition and ABTS oxidation by H_2O_2. All the mutants showed unique catalytic functions suggesting that the proximal and distal heme amino acids have vital roles in substrate binding, the electronic state and catalytic properties of the heme. The proximal histidine residue of native heme enzymes is vital for the formation of the active 5-coordinate heme structure which is necessary for their catalytic functions. Changes in the proximal pocket residues reduces the binding affinity of the iron protoporphyrin IX. The distal residue, tyrosine-140, plays an important role in catalysis as its mutation significantly reduces catalysis. However, the distal tyrosine residue can be replaced with a histidine to create a heme protein with improved the catalytic activity.

In conclusion, this study is the first to successfully create an efficient catalase from a thermophilic protein and to establish the potentials of the wild type as a peroxidase. However, to further investigate its other catalytic potentials, oxidation reactions with ferrocyanide and guaiacol, styrene epoxidation and the sulfoxidation of methyl *p*-tolyl sulfide should be performed.

REFERENCES

Alcalde M., Ferrer. M. (2006). Environmental biocatalysis: from remediation with enzymes to novel green processes. *Trends Biotechnol, 24*(6), 281-287.

Antonini E., and Brunori M. (1971). Hemoglobin and Myoglobin in Their Reactions with Ligands. *21*, 436.

Aono S, Kato T., et al. (2002). Resonance Raman and Ligand Binding Studies of the Oxygen-Sensing Signal Transducer Protein HemAT from Bacillus subtilis. *J. Biol. Chem., 277*, 13528-13538.

Asano Y., Yasuda T., et al. (1982). Microbial-Degradation of Nitrile Compounds 7. A New Enzymatic Method of Acrylamide Production. *Agric Biol Chem, 46*, 1183-1189.

Barr I, and Guo F. (2015). Pyridine Hemochromagen assay for Determining the Concentration of Heme in Purified Protein solutions. *HHS. Pub. Acc., 5(18).*

Bistolas N., Wollenberger U., et al. (2005). Cytochrome P450 Biosensors-a Review. *Biosens Bioelectron. , 20*, 2408-23.

Boon E.M., Downs A., and Marcey D. (2007). Catalase: H_2O_2: H_2O_2 Oxidoreductase. *Cat. Struct. Tut. Text.*

Boon E.M., and Marletta M. A. (2005). Ligand Discrimination in Soluble Guanylate Cyclase and the H-NOX Family of Heme Sensor Proteins. (S. Direct, Ed.) *Curr. Opin. Chem. Biol., 9*, 441-446. doi:10.1016/j.cbpa.2005.08.015.

Boon E.M., Huang S., and Marletta M.A. (2005). A Molecular Basis for NO Selectivity in Soluble Guanylate Cyclase. *Nat Chem Biol, 1*, 53-59.

Bornscheuer U.T., Pohl M. (2001). Improved Biocatalysts by Directed Evolution and Rational Protein Design. *Curr Opin Chem Biol., 5*, 137-143.

Bornscheuer U.T., and Kazlauskas R.J. (1999). Hydrolases in Organic Synthesis Regio- and Stereoselective Biotransformations Using Different Hydrolases. *Wiley-Blackwell.*

Bradshaw W.H., Conrad H.E. (1959). Microbiogical Degradation of (+)-Camphor. *J. Am. Chem. Soc., 81.*, 5007.

Carlsen C.U., Skougaard I.M., and Skibsted L.H. (2003). Pseudoperoxidase Activity of Myoglobin: Kinetics and Mechanismof the Peroxidase Cycle of Myoglobin with H2O2 and 2,2-Azino-bis(3-ehtylbenzthiazoline-6-sulfonate) as substrates. *J. Agric. Food Chem., 51*, 5815-5823.

Carlson H.K., Vance R.E. (2010). H-NOX Regulation of c-di-GMP Metabolism and Biofilm Formation in Legionella pneumophila. *Mol Microbiol., 77*, 930-942.

Cedrone F, Menez A. (2000). Tailoring New Enzyme Functions by Rational Design. *Curr Opin Struct Biol, 10*, 405-410.

Chen L., and Waxman D.J (2002). Cytochrome P450 gene-directed enzyme prodrug therapy (GDEPT) for cancer. *Curr Pharm Des., 8*, 1405-1416.

Crump S., Rozzell J.D. (1992). Biocatalytic Production of Amino Acids By Transamination. In Biocatalytic Production of Amino Acids and Derivatives. 43–58.

Dalboge H., and Lange L. (1998). Using Molecular Techniques to Identify New Microbial Biocatalysts. . *Trends Biotechnol., 16*(6), 265-272.

Denninger J.W., and Marletta M.A. (1999). Guanylate Cyclase and he NO/cGMP Signaling Pathway. *Biochim Biophys Acta., 1411*, 334-350.

Diaz J.E., Lin C.-J., et al. (2011). Computational design and selections for an engineered, thermostable terpene synthase. *Protein Sci., 20*(9).

Dincer A., Telefoncu. A. (2007). Improving the Stability of Cellulase by Immobilization on Modified Polyvinyl Alcohol Coated Chitosan Beads. *J Mol Catal B Enzym*, 10-14.

Drauz, K., Groger H., and May Q. (2012). *Enzyme Catalysis in Organic Synthesis* (3rd ed.). Wiley-VCH: Weinheim.

Elleuche S., Schroder C., et al. (2014). Extremozymes-Biocatalysts with Unique Properties from Extremophilic Microorganisms. *Curr Opin Biotechnol. , 29C*, 116-123.

Faber K. (1997). *Biotransformations. In Organic Chemistry: A Textbook.* Berlin, Germany: Springer-Verlag.

Falck J.R., Reddya Y.K., et al. (2001). Practical enantiospecific syntheses of 14,15-EET and leukotoxin B (vernolic acid). *Tetrahedron Letters., 42*, 4131-33.

Fuji T., Fuji Y., et al (2009). Efficient biotransformations using Escherichia coli with tolC acrAB mutations expressing cytochrome P450 genes. *Biosci Biotechnol Biochem., 73*, 805-10.

Gajhede M. (2001). *Handbook of metalloproteins.* (H. R. Messerschmidt A., Ed.) Chichester.

Gillam E.M., and Guengerich F.P. (2001). Exploiting the versatility of human cytochrome P450 enzymes: the promise of blue roses from biotechnology. *IUBMB Life., 52*, 271-277.

Gilles-Gonzalez M.A., Ditta G.S., and Helinski D.R. (1991). A Hemoprotein with Kinase Activity Encoded bythe Oxygen Sensor of Rhizobium meliloti. *Nature, 350*, 170-172.

Glick B.R., Pasternak J.J. (2010). *Molecular Biotechnology: Principles and Applications of Recombinant DNA* (4th ed.). Washington, DC: ASM Press.

Gong W, Hao B.R., et al. (1998). Structure of a biological oxygen sensor: a new mechanism for heme-driven signal transduction. *Proc. Natl. Acad. Sci USA., 95*(26), 15177-15182.

Green M.T. (2000). Imidazole-ligated compound I intermediates: the effects of hydrogen bonding. *J. Am. Soc., 122*(39), 9495-9499.

Guo W.W., Wan D., et al. (2012). Unusual Peroxide Activity of a Myoglobin Mutant with Two Distal Histidines. *Chin Chem Letters, 23*, 741-744.

Hare J.M., and Colucci W.S. (1995). Role of Nitric Oxide in the Regulation of Myocardial Function. *Prog Cardiovasc Dis., 38*, 155-166.

Harris J.L., and Craik C.S. (1998). Engineering Enzyme Specificity. *Curr Opin Biol, 2,* 127-132.

Henares B.M., Xu Y., and Boon E.M. (2012). Discovery of a Nitric Oxide Responsive Quorum Sensing Circuit in Vibro harveyi. . *ACS Chem Biol., 7,* 1331-1336.

Homaei A.A., Sariri R., et al. (2013). Enzyme immobilization: an update. *J Chem Biol., 6*(4), 185-205.

Hou S, Larsen R.W., et al. (2000). Myoglobin-Like Aerotaxis Transducers in Archaea and Bacteria. *Nature, 403,* 540-544.

Hunt S. (2001). Technology evaluation: MetXia-P450. *Curr. Opin. Mol. Ther., 3,* 595-598.

Isaac I.S., Dawson J.H. (1999). Haem Iron-Containing Peroxidases. . *Essays Biochem., 39,* 51-69.

Ishaq R., Naf C., et al. (2003). PCBs, PCNs, PCDD/Fs, PAHs and Cl-PAHs in Air and Water Particulate Samples--Patterns and Variations. *Chemosphere., 50,* 1131-50.

Isin E.M., and Guengrich F.P. (2007). Complex Reactions Catalyzed by Cytochrome P450 Enzymes. *BBA., 1770,* 314-329.

Iyer L.M., Anantharaman V., and Aravind L. (2003). Ancient Conserved Domains Shared by Animal Soluble Guanylyl Cyclases and Bacterial Signaling Proteins. *BMC Genomics., 4*(1), 5.

Jain R, and Chan M.K. (2003). Mechanism of Ligand Discrimination by Heme Proteins. *J. Biol. Inorg. Chem., 8,* 1-11.

Johannes T., Simurdiak M.R. and Zhao H. (2006). Biocatalysis. *Encycl. Chem. Proc.,* 101-110.

Joo H., Lin Z., and Arnold F.H. (1999). Laboratory Evolution of Peroxide-Mediated Cytochrome P450 Hydroxylation. *Nature., 399,* 670-672.

Jounaidi Y., Hecht J.E., and Waxman D.J. (1998). Retroviral transfer of human cytochrome P450 genes for oxazaphosphorine-based cancer gene therapy. *Cancer Res., 58,* 4391-401.

Jounaidi Y., and Waxman D.J. (2001). Frequent, Moderate-Dose Cyclophosphamide Administration Improves the Efficacy of Cytochrome P-450/Cytochrome P450 Reductase-Based Cancer Gene Therapy. *Jounaidi Y, Waxman DJ, 61*, 4437-4444.

Jounaidi Y., and Waxman D.J. (2004). Use of Replication-Condition Adenovirus as a Helper System to Enhance Delivery of P450 Prodrug-Activation Genes in Cancer Therapy. *Cancer Res. , 64*, 292-303.

Jouve H.M., Andreoletti P., et al. (1997). Structural Analysis of Compound I in Hemoproteins: Study on Proteus Mirabilis Catalase. *Biochimie., 63,* 810-816.

Kadnikova E.N., and Kostic N.M. (2002). Oxidation of ABTS by Hydrogen Peroxide Catalyzed by Horseradish Peroxidase Encapsulated into Sol-Gel Glass. Effects of Glass Matrix on Reactivity. *J Mol Catalysis B: Enzymatic, 18*, 39-48.

Kaim W., and Schwederski B. (1996). *Bioinorganic Chemistry: Inorganic Elements in the Chemistry of Life.* Chichester: Wiley.

Karow D.S., Pan D., et al. (2004). Spectroscopic Characterization of the Soluble Guanylate Cyclase-like Heme Domains from Vibrio cholerae and Thermoanaerobacter tengcongensis. *Biochemistry., 43*(31), 10203-10211.

Kim D., and Guengerich F.P. (2004). Enhancement of 7-Methoxyresorufin O-Demethylation Activity of Human Cytochrome P450 1A2 by Molecular Breeding. *Arch Biochem Biophys., 432*, 102-108.

Kim D., and Guengerich F.P. (2005). Analysis of Coumarin 7-Hydroxylation Activity of Cytochrome P450 2A6 Using Random Mutagenesis. *J Biol Chem., 280*, 40319-27.

Kumar S. (2010). Engineering Cytochrome P450 Biocatalysts for Biotechnology, Medicine, and Bioremediation. *Expert Opin Drug Metab Toxicol., 2*, 115-131.

Kurt and Faber. (Ed.). (2011). *Biotransformations in Organic Chemistry* (6th ed.). Heidelberg: Springer.

Lamb D.C., Guengerich F.P., et al. (2006). Streptomyces P450s as a Model for Drug Discovery. *Expert Opin. Drug Metab. Toxicol. , 2*, 27-40.

Lee S.G., and Henthorn D. (2012). *Materials in Biology and Medicine (Green Chemistry and Chemical Engineering).* CRC Press.

Lemiere G.L., Lepoiure J.A. and Alderweireldt F.C. (1985). Hlad-catalyzed oxidations of alcohols with acetaldehyde as a coenzyme recycling substrate. *Science Direct., 29*(37), 4527-4528.

Li H. (2001). Handbook of metalloproteins. In H. R. Messerschmidt A. (Ed.). Chichester.: Wiley.

Li T., Bonkovsky H. L. and Guo J-T. (2011). Structural Analysis of Heme Proteins: Implications. *BMC. Struc. Biol., 11*(13).

Liddington R., Derewenda Z., et al. (1992). High-Resolution Crystal Structures oand Comparisons of T-State Deoxyhaemoglobin and Two Liganded T-State Haemoglobins: T(alpha-oxy)haemoglobin and T(met)haemoglobin. . *J. Mol.Biol. , 228*, 551-579.

Liese A., Seelbach K., and Wandrey C. (2002). Industrial Biotransformations. *Org Proc Res Dev., 6*(1), 86-87.

Lin Y-W., Yeung N., et al. (2010). Roles of Glutamates and metal Ions in a Rationally Designed Nitric Oxide Reductase Based on Myoglobin. *Proc. Natl. Acad. Sci., 109*(19), 8581-8586.

Lin Y-W., Yeung N., Gao Y-G.. et al. (2010). Introducing a 2-His-1-Glu Non-Heme Iron Center into Myoglobin. *J Am Chem Soc., 132*(29), 9970-9972.

Liu W., and Wang P. (2007). Cofactor Regeneration for Sustainable Enzymatic Biosynthesis. *Biotechnol adv., 25,* 369-384.

Lu Y., Berry S.M., and Pfister T.D. (2001). Engineering Novel Metalloproteins: Design of Metal-Binding Sites into Native Protein Scaffolds. *Chem. Rev., 101*, 3047-3080.

Lu Y., Yeung N., et al. (2009). Design of Functional Metalloproteins. *Nature., 460*(7257), 855-862.

Marletta M.A., Plate L. (2012). Nitirc Oxide Modulates Bacterial Biofil Formation Through a Multicomponent Cyclic-di-GMP Signaling Network. . *Mol Cell., 46*, 449-460.

Maté M.J., Bravo J., et al. (2001). *Handbook of Metalloproteins.* (H. R. Messerschmidt A., Ed.) Chichester.

Matsui T., Shingo N., et al. (1996). Preparation and Reactions of Myoglobin Mutants Bearing Both Proximal Cysteine Ligand and Hydrophobic Distal Cavity: Protein Models for the Active Site of P-450. *Biochemistry., 35,* 13118-13124.

Matsui T., Ozaki S.I., et al. (1999). Effects of the Location of Distal Histidine in the Reaction of Myoglobin with Hydrogen Peroxide. *J Biol Chem., 274*, 2838-2844.

Matsuo T., Fukumoto K., et al (2011). Precise Design of Artificial Cofactors for Enhancing Peroxidase Activity of Myoglobin: Myoglobin Mutant H64D Reconstituted with a “Single-Winged Cofactor” Is Equivalent to Native Horseradish Peroxidase in Oxidation Activity. *Chem. Asian J., 6*(9), 2491-2499.

Moffet D.A., Certain L.K. (2000). Peroxidase Activity in Heme Proteins Derived from a Designed Combinatorial Library. *J. Am. Chem. Soc., 31*(122), 7612-7613.

Mohammad N.R., Marzuki N.H.C., et al. (2015). An overview of technologies for immobilization of enzymes and surface analysis techniques for immobilized enzymes. *Biotechnol Biotechnol Eguip., 29*(2), 205-220.

Monson E.K, Weistein M., et al. (1992). The FixL Protein of Rhizobium melitoti Can be Separated into a Heme-Binding Oxygen-Sensing Domain and a Functional C-Terminal Kinase Domian. *Proc. Natl. Acad. Sci. U.S.A., 89*, 4280-4284.

Moore G.R., and Pettigrew G.W. (1990). Cytochromes C;. (Springer-Verlag., Ed.)

Morant M., Bak S., et al. (2003). Plant cytochromes P450: Tools for Pharmacology, Plant Protection and Phytoremediation. *Curr Opin Biotechnol. , 14*, 151-162.

Oezguen N., Kumar S., et al. (2008). Identification and analysis of conserved motifs in cytochrome P450 family 2: Functional role of a motif 187RFDYKD192 in P450 2B enzymes. *J Biol Chem., 283*, 21808-16.

Olea C., Boon M.E., et al. (2008). Probing the Function of Heme Distortion in the H-NOX Family. *ACS Chem Biol., 3*, 703-710.

Olson J, Eich R., et al. (1999). Protein Engineering Strategies for Designing More Subtle Hemoglobin-Based Blood Sunstitutes. *Artif. Cells Blood Substit. Immobil. Biotechnol., 25*(1-2), 227-241.

Ortiz de Montellano P.R., and Nelson S.D. (2011). Rearragement Reactions Catalyzed by Cytochrome P450s. *Arch. Biochem. Biophys.*, 95-110.

Park S.Y., Shimizu H., et al. (1997). Crystal Structure of Nitric Oxide Reductase from Denitrifying Fungus Fusarium Oxysporum. *Nat. Struct. Biol. , 4*, 827-832.

Patel R.N. (2000). Steroselective Biocatalysis. (R. N. Patel, Ed.) *CRC Press.*

Pellequer J.L, Brudler R., and Getzoff E.D. (1999). Biological Sensors: More than One Way to Sense Oxygen. . *Curr. Biol., 9*, R416-418.

Pellicena P., Karow D.S., et al. (2004). Crystal Structure of an Oxygen-Binding Heme Domain Related to Soluble Guanylate Cyclases. *Proc Natl Acad Sci U.S.A., 101*, 12854-12859.

Pfister T.D., Ohki T., et al. (2005). Monooxygenation of an Aromatic Ring by F43W/H64D/V68I Myoglobin Mutant and Hydrogen Peroxide. *J Biol Chem., 280*(1), 12858-12866.

Plate L., and Marletta M.A. (2013). Nitric Oxide-Sensing H-NOX Proteins Govern Bacterial Communal Behavior. *Trends Biochem Sci., 38*(11), 566-575.

Pollard D.J., and Woodley J.M. (2007). Biocatalysis for Pharmaceutical Intermediates: The Future is Now. *Trends. Biotechnol. 25*(2), 66-73.

Poulos T.L. (1996). Ligands and Eelectrons and Haem Proteins. *Nat. Struct. Biol., 3*, 401-403.

Poulos T.L. (2014). Heme Enzyme Structure and Function. *Chem Rev, 114*(7), 3919-3962.

Reetz, and Manfred T. (2013). Biocatalysis in Organic Chemistry and Biotechnology: Past, Present, and Future. *Journal of American Chemical Society*(135), 12480−12496.

Rodgers K.R. (1999). Heme-based sensors in biological systems. *Curr. Opin. Chem. Biol., 3*(2), 158-67.

Rothlisberger D., Khersonsky O., et al. (2008). Kemp Elimination Catalysts by Computational Enzyme Design. *Nature. 453*(7192), 190-5.

Rosenfeld. (2001). *Handbook of Metalloproteins.* (H. R. Messerschmidt A., Ed.) Chichester.: Wiley.

Roy P., and Waxman D.J. (2006). Activation of oxazaphosphorines by cytochrome P450: application to gene-directed enzyme prodrug therapy for cancer. *Toxicology in Vitro., 20*, 176-186.

Rozzell J.D. (1999). Commercial Scale Biocatalysis: Myths and Realities. *Bioorg. Med. Chem., 7*(10), 2253-2261.

Rydberg P., Sigfridsson E., and Ryde U. (2004). On the Role of the Axial Ligand in Heme Proteins: a Theoretical Study. *J. Biol. Inorg. Chem., 9*(2), 203-223.

Sakaki T., Shinkyo R., et al. (2002). Biodegradation of Polychlorinated Dibenzo-p-dioxins by Recombinant Yeast Expressing Rat CYP1A Subfamily. *Arch Biochem Biophys., 401*, 91-98.

Sato H., Hayashi T., et al. (2004). Hybridization of Modified-Heme Reconstitution and Distal Histidine Mutation to Functionalize Sperm Whale Myoglobin. *J. Am Chem. Soc., 126*(2), 436-437.

Schmid A., Dordick J.S., et al. (2001). Industrial Biocatalysis Today and Tomorrow. *409*, 258-268.

Schmidt P., Rothkegel C., et al. (2005). Residues Stabilizing the Heme Moiety of the Nitric Oxide Sensor Soluble Guanylate Cyclase. . *Eur J Pharmacol. , 513*, 67-74.

Schmidt P.M., Schramm M., et al. (2004). Identification of Residues Crucially Involved in the Binding of the Heme Moiety of Soluble Guanylate Cyclase. *J Biol Chem., 279*(4), 3025-32.

Servi S. (1990). Baker's Yeast as a Reagent in Organic Synthesis. *Synthesis., 1*, 1-25.

Shah A.M., and MacCarthy P.A. (2000). Paracrine oand Autocrine Effects of Nitric Oxide on Myocardial Function. *Pharmacol Ther., 86*, 49-86.

Shelver D., Kerby R.L., et al. (1997). CooA, a CO-Sensing Transcription Factor from Rhodospirillum rubrum, is a CO-Binding Heme Protein. *Proc Natl Acad Sci., 94*, 11216-11220.

Shinkyo R., Kamakura M., et al. (2006). Biodegradation of Dioxins by Recombinant Escherichia coli Expressing Rat CYP1A1 or its Mutant. . *Appl Microbiol Biotechnol., 72*, 584-90.

Shoemaker H.E., Mink D., and Wubbold M.C. (2003). Dispelling the Myths--Biocatalysis in Industrial Synthesis. *Sci.* 1694-1697.

Shyadehi A.Z., Lamb D.C. , et al. (1996). The Mechanism of the Acyl-Carbon Bond Cleavage Reaction Catalyzed by Recombinant Sterol 14 Alpha-Demethylase of Candida albicans. *J. Biol. Chem.*, 12445-12450.

Siegel J.B., Zanghellini A., et al. (2010). Computational Design of an Enzyme Catalyst for a Stereoselective Bimolecular Diels-Alder Reaction. *Sci. 329*(5989), 309-13.

Sigmam J.A., Kim H.K., et al. (2003). The Role of Copper and Protons in Heme-Copper Oxidases: Kinetic Study of an Engineered Heme-Copper Center in Myoglobin. *Proc. Natl Acad. Sci., 100*, 3629-3624.

Sonomoto K., Hoq M.M., et al. (1983). 11beta-Hydroxylation of Cortexolone (Reichstein Compound S) to Hydrocortisone by Curvularia lunata Entrapped in Photo-Cross-Linked Resin Gels. *Appl Environ Microbiol, 45*, 436-443.

Spahn C., and Minteer S.D. (2008). Enzyme Immobilization in Biotechnology. *Rec. Pat. Eng.* 195-200

Sundaramoorthy M. (2001). *Handbook of Metalloproteins.* (H. R. Messerschmidt A., Ed.) Chichester.: Wiley.

Tiwari M.K., Sing R., et al. (2012). Computational Approaches for Rational Design of Proteins with Novel Functionalities. (S. Direct, Ed.) *Computational and Structural Biotechnology Journal, 2*(3).

Toda N., and Okamura T. (2003). The Pharmacology of Nitric Oxide in the Peripheral Nervous System of Blood Vessels. *Pharmacol Re., 55*, 271-324.

Trudeau D.L., Lee T.M., and Arnolf F.H, et al. (2014). Engineered thermostable fungal cellulases exhibit efficient synergistic cellulose hydrolysis at elevated temperatures. *Biotechnol Bioeng., 111*(12), 2390-7.

Underbakke E.S., Surmeli N.B., et al. (2013). Nitirc Oxide Signaling. *3,* 241-262.

Urlacher V.B., and Girhard M, (2012). Cytochrome P450 Monooxygenases: An Update on Perspectives for Synthetic Application. *Trend. Biotechnol.*, *30*(1), 26-36.

Wandrey C., Liese A., and Kihumbu D. (2000). Industrial biocatalysis: Past, present, and future. *Org. Proc. Res. Dev. 4*(4), 286-290.

Walsh M.E., Kritsis P., et al. (2000). Catalytic Reductive Dehalogenation of Hexachloroethane by Molecular Variants of Cytochrome P450CAM (CYP101). *Eur J Biochem. , 67*, 5815-20.

Wang Y. (2010). H-NOX-Mediated Nitric Oxide Sensing Modulates Symbiotic Colonization by Vibrio fischeri. . *Proc Natl Acad Sci. U.S.A., 107,* 8375-8380.

Watanabe Y., Nakajima H., et al. (2007). Reactivities of Oxo and Peroxo Intermediates Studied by Hemoprotein Mutants. *Acc Chem Res.*, *40*, 554-562.

Wittenberg J., and Wittenberg B. (1990). Mechanisms of Cytoplasmic Hemoglobin and Myoglobin Function. *Annu. Rev. Biophys. Biophys. Chem.*, *19*, 217-41.

Wolfenden R., Snider M.J. (2001). The Depth of Chemical Time and the Power of Enzymes as Catalysts. *Acc Chem Res*, *34*, 938-945.

Woycechowsky K.J., Vamvaca K., et al. (2007). Novel Enzymes Through Design and Evolution. *Adv Enzymol Relat Areas Mol Biol.*, *75*, 241-294.

Yeung N., Lin Y.W., et al. (2009). Rational Design of a Structural and Functional Nitric Oxide Reductase. *Nature.*, *462*(7276), 1079-1082.

Zerbe K., Pylypenko O., et al. (2002). Crystal Structure of OxyB, a Cytochrome P450 Implicated in an Oxidative Phenol Coupling Reaction During Vancomycin Biosynthesis. *J. Biol. Chem., 277*, 47476-47485.

Zerbe K., Woithe K., et al. (2004). An Oxidative Phenol Coupling Reaction Catalyzed by OxyB, a Cytochrome P450 from the Vancomycin-Producing Microorganism. *Angew. Chem. Int. Ed., 43*, 6709-6713.

Zhao Y.H., and Halpert J.R. (2007). Structure-Function Analysis of Cytochromes P450 2B. *Arch Biochem Biophys., 1770*, 402-412.

APPENDIX A

AMINO ACID SEQUENCES

Wild type *Tt*H-NOX:

HMKGTIVGTWIKTLRDLYGNDVVDESLKSVGWEPDRVITPLEDIDDDEV RRIFAKVSEKTGKNVNEIWREVGRQNIKTFSEWFPSYFAGRRLVNFLMMMDEV HLQLTKMIKGATPPRLIAKPVAKDAIEMEYVSKRKMYDYFLGLIEGSSKFFKEEI SVEEVERGEKDGFSRLKVRIKFKNPVFEYKKNLEHHHHHH

H102C *Tt*H-NOX:

HMKGTIVGTWIKTLRDLYGNDVVDESLKSVGWEPDRVITPLEDIDDDEVRRIFA KVSEKTGKNVNEIWREVGRQNIKTFSEWFPSYFAGRRLVNFLMMMDEVCLQL TKMIKGATPPRLIAKPVAKDAIEMEYVSKRKCMIIFWALKAAAIFQRRNVEKT WRKNGFGLLKCVLIKPGGWIKNLEHHHHHH

H102Y *Tt*H-NOX:

HMKGTIVGTWIKTLRDLYGNDVVDESLKSVGWEPDRVITPLEDIDDDEVRRIFA KVSEKTGKNVNEIWREVGRQNIKTFSEWFPSYFAGRRLVNFLMMMDEVYLQL TKMIKATPPRLIAKPVAKDAIEMEYVSKRKMYDYFLGLIEGSSKFFKEEISVEEV ERGEKDGFSRLKVRIKFKNPVFEYKKNLEHHHHHH

Y140A *Tt*H-NOX:

HMKGTIVGTWIKTLRDLYGNDVVDESLKSVGWEPDRVITPLEDIDDDEVRRIFA KVSEKTGKNVNEIWREVGRQNIKTFSEWFPSYFAGRRLVNFLMMMDEVHLQL TKMIKGATPPRLIAKPVAKDAIEMEYVSKRKMYDAFLGLIEGSSKFFKEEISVEE VERGEKDGFSRLKVRIKFKNPVFEYKKNLEHHHHHH

Y140H *Tt*H-NOX:

HMKGTIVGNWIKTLRDLYGNDVVDESLKSVGWEPDRVITPLEDIDDDEVRRIFA KVSEKTGKNVNEIWREVGRQNIKTFSEWFPSYFAGRRLVNFLMMMDEVHLQL TKMIKGATPPRLIAKPVAKDAIEMEYVSKRKMYDHFLGLIEGSSKFFKEEISVEE VERGEKDGFSRLKVRIKFKNPVFEYKKNLEHHHHHH

APPENDIX B

VECTOR MAP

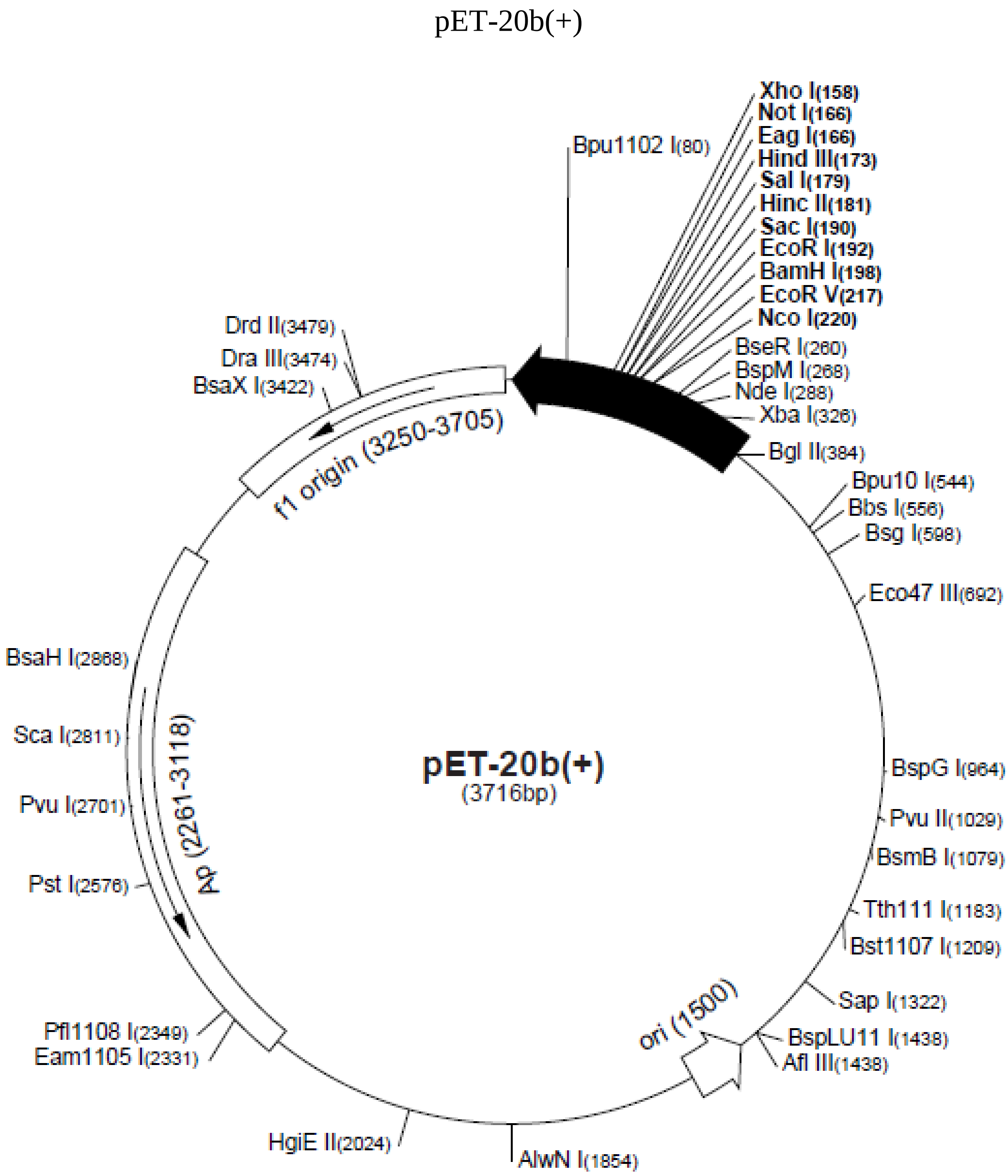

Figure B.1. pET-20b vector map.